





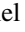
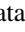






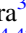

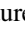
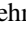
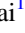


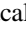




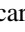

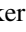




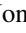

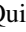

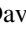








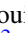

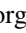
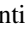


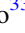

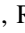


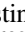
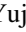





The TESS-Keck Survey: * Science Goals and Target Selection

Ashley Chontos^{1,40} , Joseph M. Akana Murphy^{2,40} , Mason G MacDougall³ , Tara Fetherolf^{4,41} , Judah Van Zandt³ ,
 Ryan A. Rubenzahl^{5,40} , Corey Beard⁶ , Daniel Huber¹ , Natalie M. Batalha² , Ian J. M. Crossfield⁷,
 Courtney D. Dressing⁸ , Benjamin Fulton⁹ , Andrew W. Howard⁵ , Howard Isaacson^{8,10} , Stephen R. Kane⁴ ,
 Erik A. Petigura³ , Paul Robertson⁶ , Arpita Roy^{11,12} , Lauren M. Weiss¹ , Aida Behrard^{13,40} , Fei Dai¹³ ,
 Paul A. Dalba^{4,14,42} , Steven Giacalone⁸ , Michelle L. Hill⁴ , Jack Lubin⁶ , Andrew Mayo^{8,40} , Teo Močnik¹⁵ ,
 Alex S. Polanski⁷, Lee J. Rosenthal⁵ , Nicholas Scarsdale² , Emma V. Turtelboom⁸ , George R. Ricker¹⁶ ,
 Roland Vanderspek¹⁶ , David W. Latham¹⁷ , Sara Seager^{16,18,19} , Joshua N. Winn²⁰ , Jon M. Jenkins²¹ ,
 Samuel N. Quinn¹⁷ , Natalia M. Guerrero^{16,22} , Karen A. Collins¹⁷ , David R. Ciardi²³ , Avi Shporer¹⁶ ,
 Robert F. Goetze¹⁶ , Alan M. Levine¹⁶ , Eric B. Ting²¹ , Allyson Bieryla¹⁷ , Kevin I. Collins²⁴ , John F. Kielkopf²⁵ ,
 Khalid Barkaoui^{18,26,27} , Paul Benni²⁸ , Emma Esparza-Borges^{27,29} , Dennis M. Conti³⁰ , Matthew J. Hooton³¹ ,
 Taiki Kagetani³² , Didier Laloum³⁰, Giuseppe Marino^{33,34} , Bob Massey³⁵ , Felipe Murgas^{27,29} , Riccardo Papini^{30,33},
 Richard P. Schwarz³⁶ , Gregor Srdoc³⁷, Chris Stockdale³⁸ , Gavin Wang³⁹ , Justin M. Wittrock²⁴ , and Yujie Zou³² 

¹ Institute for Astronomy, University of Hawai'i, 2680 Woodlawn Drive, Honolulu, HI 96822, USA; achontos@hawaii.edu

² Department of Astronomy and Astrophysics, University of California Santa Cruz, Santa Cruz, CA 95064, USA

³ Department of Physics and Astronomy, University of California Los Angeles, Los Angeles, CA 90095, USA

⁴ Department of Earth and Planetary Sciences, University of California, Riverside, CA 92521, USA

⁵ Department of Astronomy, California Institute of Technology, Pasadena, CA 91125, USA

⁶ Department of Physics and Astronomy, University of California Irvine, Irvine, CA 92697, USA

⁷ Department of Physics and Astronomy, University of Kansas, 1082 Malott, 1251 Wescoe Hall Drive, Lawrence, KS 66045, USA

⁸ Department of Astronomy, University of California Berkeley, Berkeley, CA 94720, USA

⁹ NASA Exoplanet Science Institute/Caltech-IPAC, MC 314-6, 1200 E California Boulevard, Pasadena, CA 91125, USA

¹⁰ Centre for Astrophysics, University of Southern Queensland, Toowoomba, QLD, Australia

¹¹ Space Telescope Science Institute, 3700 San Martin Drive, Baltimore, MD 21218, USA

¹² Department of Physics and Astronomy, Johns Hopkins University, 3400 N Charles Street, Baltimore, MD 21218, USA

¹³ Division of Geological and Planetary Science, California Institute of Technology, Pasadena, CA 91125, USA

¹⁴ Department of Astronomy and Astrophysics, University of California, Santa Cruz, CA 95064, USA

¹⁵ Gemini Observatory/NSF's NOIRLab, 670 N. A'ohoku Place, Hilo, HI 96720, USA

¹⁶ Department of Physics and Kavli Institute for Astrophysics and Space Research, Massachusetts Institute of Technology, 77 Massachusetts Avenue, Cambridge, MA 02139, USA

¹⁷ Center for Astrophysics | Harvard & Smithsonian, 60 Garden Street, Cambridge, MA 02138, USA

¹⁸ Department of Earth, Atmospheric and Planetary Sciences, Massachusetts Institute of Technology, 77 Massachusetts Avenue, Cambridge, MA 02139, USA

¹⁹ Department of Aeronautics and Astronautics, MIT, 77 Massachusetts Avenue, Cambridge, MA 02139, USA

²⁰ Department of Astrophysical Sciences, Princeton University, 4 Ivy Lane, Princeton, NJ 08544, USA

²¹ NASA Ames Research Center, Moffett Field, CA 94035, USA

²² Department of Astronomy, University of Florida, Gainesville, FL 32611, USA

²³ Caltech/IPAC-NASA Exoplanet Science Institute, 770 S. Wilson Avenue, Pasadena, CA 91106, USA

²⁴ George Mason University, 4400 University Drive, Fairfax, VA 22030 USA

²⁵ Department of Physics and Astronomy, University of Louisville, Louisville, KY 40292, USA

²⁶ Astrobiology Research Unit, Université de Liège, 19C Allée du 6 Août 000 Liège, Belgium

²⁷ Instituto de Astrofísica de Canarias (IAC), E-38205 La Laguna, Tenerife, Spain

²⁸ Acton Sky Portal private observatory, Acton, MA, USA

²⁹ Departamento de Astrofísica, Universidad de La Laguna (ULL), E-38206 La Laguna, Tenerife, Spain

³⁰ American Association of Variable Star Observers, 49 Bay State Road, Cambridge, MA 02138, USA

³¹ Physikalisches Institut, Universität Bern, Gesellschaftsstrasse 6, 3012, Bern, Switzerland

³² Department of Multi-Disciplinary Sciences, Graduate School of Arts and Sciences, The University of Tokyo, 3-8-1 Komaba, Meguro, Tokyo 153-8902, Japan

³³ Wild Boar Remote Observatory, San Casciano in val di Pesa, I-50026 Firenze, Italy

³⁴ Gruppo Astrofili Catanesi, via Milo 28, I-95125 Catania, Italy

³⁵ Villa '39 Observatory, Landers, CA 92285, USA

³⁶ Patashnick Voorheesville Observatory, Voorheesville, NY 12186, USA

³⁷ Kotizarovci Observatory, Sarsoni 90, 51216 Viskovo, Croatia

³⁸ Hazelwood Observatory, Australia

³⁹ Tsinghua International School, Beijing 100084, People's Republic of China

Received 2021 June 10; revised 2022 March 17; accepted 2022 March 28; published 2022 May 30



Original content from this work may be used under the terms of the [Creative Commons Attribution 4.0 licence](https://creativecommons.org/licenses/by/4.0/). Any further distribution of this work must maintain attribution to the author(s) and the title of the work, journal citation and DOI.

* The TESS-Keck Survey: Science Goals and Target Selection

⁴⁰ NSF Graduate Research Fellow.

⁴¹ UC Chancellor's Fellow.

⁴² NSF Astronomy and Astrophysics Postdoctoral Fellow.

Abstract

The Kepler and TESS missions have demonstrated that planets are ubiquitous. However, the success of these missions heavily depends on ground-based radial velocity (RV) surveys, which combined with transit photometry can yield bulk densities and orbital properties. While most Kepler host stars are too faint for detailed follow-up observations, TESS is detecting planets orbiting nearby bright stars that are more amenable to RV characterization. Here, we introduce the TESS-Keck Survey (TKS), an RV program using ~ 100 nights on Keck/HIRES to study exoplanets identified by TESS. The primary survey aims are investigating the link between stellar properties and the compositions of small planets; studying how the diversity of system architectures depends on dynamical configurations or planet multiplicity; identifying prime candidates for atmospheric studies with JWST; and understanding the role of stellar evolution in shaping planetary systems. We present a fully automated target selection algorithm, which yielded 103 planets in 86 systems for the final TKS sample. Most TKS hosts are inactive, solar-like, main-sequence stars ($4500 \text{ K} \leq T_{\text{eff}} < 6000 \text{ K}$) at a wide range of metallicities. The selected TKS sample contains 71 small planets ($R_p \leq 4 R_{\oplus}$), 11 systems with multiple transiting candidates, six sub-day-period planets and three planets that are in or near the habitable zone ($S_{\text{inc}} \leq 10 S_{\oplus}$) of their host star. The target selection described here will facilitate the comparison of measured planet masses, densities, and eccentricities to predictions from planet population models. Our target selection software is publicly available and can be adapted for any survey that requires a balance of multiple science interests within a given telescope allocation.

Unified Astronomy Thesaurus concepts: [Surveys \(1671\)](#); [Telescopes \(1689\)](#); [Catalogs \(205\)](#); [Exoplanets \(498\)](#); [Exoplanet catalogs \(488\)](#); [Exoplanet systems \(484\)](#); [Fundamental parameters of stars \(555\)](#); [Observational astronomy \(1145\)](#); [Photometry \(1234\)](#); [Spectroscopy \(1558\)](#); [Radial velocity \(1332\)](#); [Exoplanet detection methods \(489\)](#)

1. Introduction

Measurements of planet sizes in combination with masses, via the transit and radial velocity (RV) methods, continues to be the most fruitful synergy for investigating the properties (in particular the bulk compositions) of exoplanets. Early landmark discoveries using both transits and RVs included the first rocky exoplanets, Kepler 10-b (Batalha et al. 2011) and CoRoT-7-b (Léger et al. 2011), as well as the density transition at $1.5 R_{\oplus}$ (Weiss & Marcy 2014), separating primarily rocky planets from the lower-density, volatile-rich, sub-Neptune-sized planets (Rogers 2015).

Kepler identified thousands of new transiting candidates (Borucki et al. 2011a, 2011b; Batalha et al. 2013; Burke et al. 2014; Mullally et al. 2015; Rowe et al. 2015; Coughlin et al. 2016; Thompson et al. 2018), but most targets were faint and therefore had limited constraints from spectroscopic RV surveys. Fortunately, this has been mitigated with TESS (Transiting Exoplanet Survey Satellite; Ricker et al. 2015), a nearly all-sky survey looking for transiting planets orbiting bright nearby stars. The first TESS discovery of a rocky super-Earth orbiting the naked-eye star π Men (Huang et al. 2018) was a prime example of the type of planet TESS was designed to detect.

A fundamental goal of exoplanet demographics is to compare observed populations of exoplanet properties to population synthesis models in order to inform planet formation theories (Mordasini 2018). This was accomplished with Kepler for planet radii (Mulders et al. 2019) and is now becoming possible for densities with TESS, but the selection function for RV follow-up is typically much more complex than for transit surveys. For example, RV surveys frequently drop stars with rapid rotation or increased stellar activity, typically on a case-by-case basis, and thus complicate the estimation of their effects on selection functions.

Large exoplanet surveys such as TESS provide the statistical insights required to test different formation and evolution theories to observed planet distributions, but the comparison hinges on the ability to understand and correct for RV survey

selection biases. Therefore, a critical ingredient for the realization of these surveys is understanding the process by which targets were initially selected. Indeed, recent ground-based TESS follow-up programs such as the Magellan-TESS Survey (MTS; Teske et al. 2021) have begun to describe target selection functions, providing a pathway to properly correct for survey biases or incompleteness.

Here, we introduce the TESS-Keck Survey (TKS), a collaboration between the California Institute of Technology, the University of California (Berkeley, Irvine, Los Angeles, Riverside, Santa Cruz), the University of Hawai'i, the University of Kansas, NASA, the NASA Exoplanet Science Institute, and the W. M. Keck Observatory. The survey is being conducted using the High-Resolution Spectrograph (HIRES), which is mounted on the Keck I telescope at the W. M. Keck Observatory on the summit of Maunakea in Hawai'i. Building on the legacies of Kepler and K2, TKS will leverage the new population of transiting planets orbiting nearby, bright stars to address major outstanding questions in exoplanet astronomy. We discuss the detailed vetting and target selection steps taken to converge on a definitive target list, including a fully automated target selection algorithm. We conclude by presenting our complete target sample and summarizing some of the general population characteristics.

2. Survey Description

2.1. TKS Science

TKS is structured around several science goals related to the compositions, architectures, and atmospheres of exoplanets (see Table 1). The following subsections provide a brief review of the science motivations for the survey.

2.1.1. Bulk Compositions

One of the most significant exoplanet discoveries by Kepler was the prevalence of planets between the sizes of Earth and Neptune (Howard et al. 2012; Fressin et al. 2013; Petigura et al. 2013). More recently, refined radius measurements identified a

Table 1
TESS-Keck Survey Science Summary

Theme	Science Case	ID ^a	Description
Bulk Compositions	Planet Radius Gap	1A	Probing compositions across the planet radius gap to constrain the physical mechanism(s) causing the bimodal radius distribution
	Stellar Flux and Gaseous Envelopes	1B	Analyzing the diversity of gaseous envelopes and their dependence on properties like stellar mass, insolation flux, activity level, and other properties
	Ultra-short-period Planets	1C	Using ultra-short-period planet compositions as a window into the refractory cores of small planets
	Habitable Zone Planets	1D	Identifying and characterizing planets orbiting in the habitable zones of their host star
	Planet–Star Correlations	1E	Exploring dependencies of bulk planet properties with different stellar properties like M_* , [Fe/H], age, etc.
Architectures and Dynamics	Distant Giants	2A	Understanding the occurrence and connection between close-in small planets and distant giant planets
	Eccentricities	2Bi	Characterizing the eccentricities of sub-Jovian planets, to elucidate the possible formation and/or evolution pathways for dynamically hot planets
	Obliquities	2Bii	Measuring spin–orbit (mis)alignments in previously unexplored regions of parameter space, to trace formation histories and past dynamical interactions
	Multis	2C	Examining the diversity and/or uniformity of properties of planets in multiplanet systems
Atmospheres		3	Identifying interesting planets amenable to atmospheric characterization using transmission and/or eclipse spectroscopy
Evolved		4	Investigating the role stellar evolution plays in shaping post-main-sequence planetary systems
Technical Outcomes	Planet Host Properties	TA	Homogeneously determining fundamental stellar properties derived from spectroscopy, asteroseismology, and astrometry
	Astrophysical Doppler Noise	TB	Studying the relationships between Doppler jitter with various stellar astrophysical processes

Note.

^a The keys in this table are used in the final TKS sample in Table 3 to identify which science case(s) each target will address.

valley in the planet distribution at a radius of $\sim 1.8 R_{\oplus}$ (Fulton et al. 2017; Fulton & Petigura 2018; Van Eylen et al. 2019).

The dominant theory for explaining the radius valley is that the two populations separated by the valley originated from a single continuous distribution and is an outcome sculpted by post-formation pathways. An example is photoevaporation, a process that strips away the atmosphere for less massive planets that receive high-energy incident flux from their host star (Owen & Wu 2013, 2017). Another mechanism is core-powered mass loss, which is also able to reproduce the observed planet radius distribution based solely on the internal cooling of a planet (Ginzburg et al. 2018; Gupta & Schlichting 2019, 2020). However, a major caveat is that the simulated planet populations used to test these theories require assumptions about the underlying mass distribution, which is degenerate with core compositions.

Multiplanet transiting systems with planets that straddle the radius valley are useful for discerning between these theories. Owen & Campos Estrada (2020) used 104 planets in 73 systems and found that only two planets were significantly ($>3\sigma$) inconsistent with the photoevaporation model. However, all planets used in the analysis were faint Kepler systems, and fewer than half of the population had actual mass constraints. TESS planets are more amenable to RV characterization and are therefore an ideal population to test these theories. A recent example was demonstrated in Cloutier et al. (2020) for TOI-732, an M dwarf with a pair of planets that straddle the gap, but more systems with a larger diversity of host star spectral types are needed.

TKS will measure precise ($>5\sigma$) masses of small planets ($<4 R_{\oplus}$) in various environments, to address some of these questions. In particular, TKS aims to probe planet compositions across the radius gap in order to constrain the underlying physical mechanism(s), including timescales for which the bimodal distribution becomes more distinct. Additionally, by targeting a range of small planets ($1 R_{\oplus} < R_p < 4 R_{\oplus}$) at various incident fluxes, TKS can test the photoevaporation hypothesis. The compositions of ultra-short-period planets ($P < 1$ day) will be used as a window into the refractory core of small planets (Dai et al. 2021). TKS will also measure masses for cooler planets in order to identify any that could have possible Earth-like compositions, especially for planets that are amenable to subsequent atmospheric characterization. Finally, TKS will make use of the entire population of small planets with precisely measured masses to investigate any dependencies or correlations of bulk planet properties with stellar properties.

2.1.2. System Architectures and Dynamics

A striking feature of the solar system is its dynamically cool architecture; i.e., planets have nearly circular, nearly coplanar orbits that are well-aligned with the rotation axis of the Sun.

In contrast, large-scale exoplanet surveys have since introduced us to planets in a rich diversity of system architectures and dynamical configurations. For instance, it is now believed that eccentricity and inclination excitation is a common outcome of various planet formation channels (Ford & Rasio 2008) or dynamical perturbation scenarios (Goldreich & Schlichting 2014). While planet detections from RV surveys

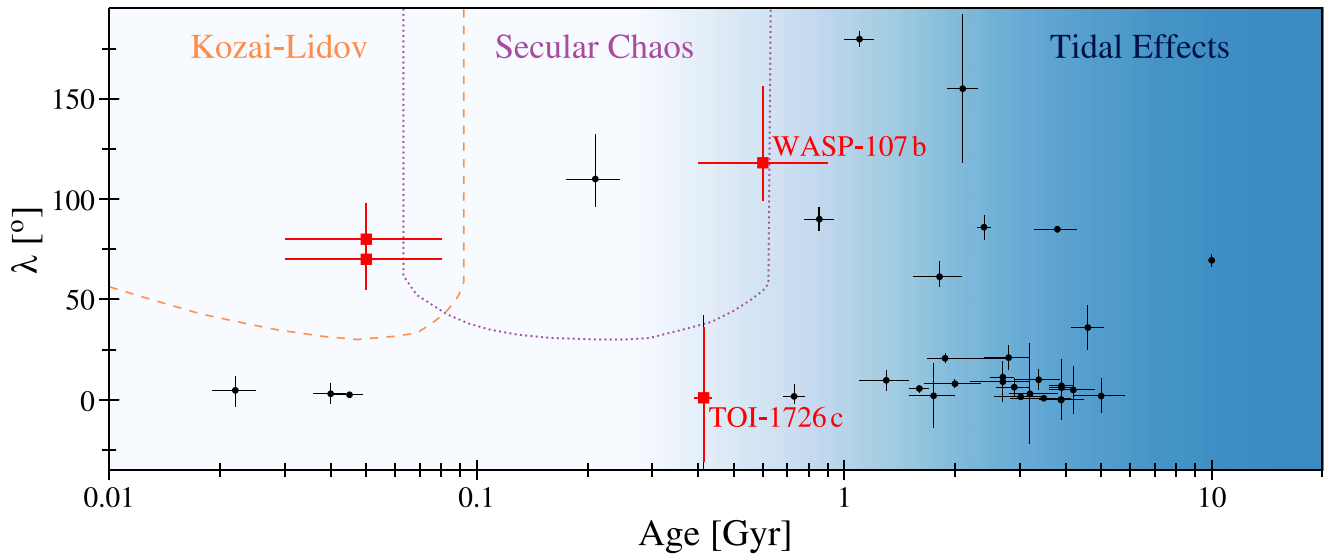


Figure 1. Stellar obliquity vs. host star age for confirmed planetary systems adapted from Zhou et al. (2020). Tidal realignment and other obliquity-exciting mechanisms such as Kozai–Lidov or secular processes operate on different timescales. Young systems with well-known ages may elucidate the relative importance of these mechanisms. TKS measurements (red) of TOI-1726c (Dai et al. 2020) and WASP-107 b (Rubenzahl et al. 2021) add crucial points to distinguish various obliquity-exciting scenarios.

have yielded well-constrained eccentricity measurements for many giant planets, sub-Jovian planet dynamics and dynamical histories remain elusive. Current observations point toward smaller planets having lower eccentricities (Van Eylen & Albrecht 2015; Van Eylen et al. 2019), but the number of such systems with precise eccentricities is low.

Another dynamical property is the obliquity, or the angle between the orbital plane and the stellar equatorial plane. There are many proposed mechanisms for spin–orbit misalignments in planetary systems that operate on different timescales (Figure 1). Some processes tilt planet orbits during the disk-hosting stage (~ 3 Myr; Batygin et al. 2011); while the Kozai–Lidov mechanism operates typically on tens of Myr timescales, depending on the system configuration (Fabrycky & Tremaine 2007). Another proposed mechanism occurs through secular interactions between planets and is expected to happen in hundreds of Myr (Wu & Lithwick 2011). Therefore, obliquity measurements of stars with well-known ages could distinguish these theories. Young planets, especially those orbiting stars with established cluster membership, have the best estimated ages and provide the strongest constraints on various obliquity-exciting theories.

TKS will shed light on these questions by measuring eccentricities and obliquities around stars of various ages. Early TKS studies have already yielded obliquities for two new systems, including a small planet in a multiplanet transiting system in the Ursa Major Moving Group (Dai et al. 2020) and the nearly pole-on, superpuff WASP-107 b (Rubenzahl et al. 2021). Additionally, TKS will increase the number of well-studied eccentric sub-Jovians by selecting high-probability eccentric candidates based on their transit durations or the “photoeccentric effect” (see Dawson & Johnson 2012). TKS will also explore the architectures of systems with multiple planets (in particular within the habitable zone) by searching for additional planets that revolve in non-transiting or longer-period orbits.

2.1.3. Spectroscopy of Exoplanet Atmospheres

Multiwavelength observations during transit and eclipse can constrain planet properties such as the admixtures of constituent gases, the presence of clouds and/or hazes, and the rate of atmospheric loss. For sub-Neptune-size planets, atmospheric observations are particularly valuable because they can help us distinguish between different possibilities for the interior composition (Rogers & Seager 2010). In turn, properties derived from these observations may be related to the location within the protoplanetary disk where the planet formed, the interaction between its atmosphere and the stellar radiation field, and planetary habitability (Mordasini et al. 2016). The number of current measurements of sub-Jovian atmospheres is limited due to the scarcity of such targets around bright stars (Crossfield & Kreidberg 2017).

With the launch of the James Webb Space Telescope (JWST; Gardner et al. 2006), mass measurements of small TESS planets that are amenable to atmospheric characterization are critical for planning future follow-up observations. Exoplanets require precise ($\geq 5\sigma$) mass measurements to break the degeneracy between surface gravity and atmospheric mean molecular weight when interpreting their transmission spectra (Batalha et al. 2019). Therefore, TKS will follow up and measure masses with the required precision ($\geq 5\sigma$) in order to identify prime targets to be later observed with JWST for atmospheric studies.

2.1.4. Evolved Host Stars

Subgiant stars are frequently avoided in exoplanet surveys, with the exception of early RV surveys that aimed to probe the occurrence rates of gas-giant planets with stellar mass (Johnson et al. 2007, 2010, 2013). For transiting planets, larger stars bias detections toward larger planets while RV measurements of subgiants tend to be noisier than those of main-sequence stars (Luhn et al. 2019, 2020). However, the fraction of the total lifetime of a star spent on the subgiant branch is comparatively

small, and therefore, a location on an HR-diagram conveniently provides a much more precise mass and age than that of a main-sequence star. Specifically in the Gaia era, the effective temperature, luminosity, and metallicity alone are sufficient to characterize a subgiant for most investigations of the planets that it hosts.

Precise ages are valuable when placing observational constraints on dynamical timescales for exoplanets. Previous studies have suggested that the dynamical timescales for processes like circularization or inward migration through tidal dissipation are strongly dependent on the scaled semimajor axis of the system (a/R_* ; see Zahn 1977; Hut 1981; Zahn 1989). Since this property is most rapidly changing for subgiant stars, stellar evolution is expected to affect tidal circularization timescales of close-in gas-giant planets, producing a transient population of mildly eccentric planets orbiting evolved stars (Villaver et al. 2014). Kepler and K2 data have yielded intriguing evidence supporting this theory, but were based on a small sample of planets (Grunblatt et al. 2018; Chontos et al. 2019). By building up a more statistically significant population of planets orbiting subgiants, TKS will be able to further investigate the role of stellar evolution in shaping post-main-sequence planetary systems.

Another advantage of studying planets orbiting evolved stars is that the likelihood of performing asteroseismology increases, since the amplitude of the oscillations increases with stellar luminosity. Ensemble studies of exoplanets orbiting asteroseismic stars have provided some of the most precise planet properties to date, revealing features like the hot sub-Neptune desert (Lundkvist et al. 2016) and the radius valley (Van Eylen et al. 2019). First examples for asteroseismology–exoplanet synergies with TESS include transiting planets around TOI 197 (Huber et al. 2019) and TOI 257 (Addison et al. 2021), as well as asteroseismic detections in solar analogs that are prime targets for future direct imaging missions (Chontos et al. 2021).

2.2. Technical Outcomes

2.2.1. Host Star Characterization

Fundamental properties of planet hosts are essential to realizing the full scientific return of TESS. High-resolution spectroscopy allows the precise determination of effective temperatures and chemical abundances, which combined with Gaia parallaxes allow the precise characterization of exoplanet host star properties such as stellar masses (Berger et al. 2018, 2020). The results of the homogeneous stellar characterization of TESS host stars using Keck/HIRES, including TESS planet hosts beyond the target sample described here, will be presented in a future study.

2.2.2. Understanding Stellar Doppler Noise

Various stellar phenomena such as spot modulation, granulation, and chromospheric activity, produce apparent RV shifts or “jitter” that compete with planetary signals and thus make more active stars unfavorable targets for precise radial velocity (PRV) work. Fortunately, TESS enables a link between photospheric variability and observed RV shifts by providing precise photometry for stars that already have long-term ground-based RV monitoring. In addition, activity studies benefit immensely when RVs and photometry are collected contemporaneously. For such data sets, jitter may be mitigated to reveal exoplanet signals that would otherwise be inaccessible

(López-Morales et al. 2016). TKS will leverage TESS to better understand the astrophysical processes causing jitter and develop techniques to mitigate and remove it.

3. Target Vetting

3.1. Photometry

All TKS targets underwent a series of vetting procedures before being selected for precise RV follow-up. Targets are drawn from the database of TESS Objects of Interest (TOI; Guerrero et al. 2021), which is publicly available.⁴³ Targets below a decl. of -30° were excluded based on Keck observability and resources. A visual magnitude cut ($V < 13$) was implemented where available; otherwise, the TESS magnitude was used ($T < 13$). Targets with a higher Gaia renormalized unit weight error⁴⁴ (RUWE > 2), indicative of an unresolved companion, were also excluded from target selection (Evans 2018; Belokurov et al. 2020). Additional cuts were implemented to remove candidate hosts with $T_{\text{eff}} > 6500$ K and planet candidates with $R_p > 22 R_\oplus$.

All remaining targets were individually vetted by a member of the TKS photometric “tiger” team. Data validation (DV) products from the SPOC (Science Processing Operations Center; Jenkins et al. 2016; Twicken et al. 2018; Li et al. 2019) and the QLP (Quick Look Pipeline; Huang et al. 2020a, 2020b) pipelines were inspected, ruling out possible false-positive scenarios. Close attention was given to metrics such as the ghost diagnostic and odd–even transit differences. Additionally, TOIs with transit detection signal-to-noise ratios (S/N) less than 10 were excluded because the planet radius uncertainty would dominate the uncertainty in the bulk density for such targets.

A special set of selection rules were implemented for out-of-transit centroid offsets, where targets with a $< 3\sigma$ offset would always pass this vetting step. For centroid offsets between 3σ and 5σ , a target would still pass if the offset was $< 21''$, unless the centroid offset was at a nearby star according to the DV report. For $> 5\sigma$ offsets, the target would still pass if $T < 7.5$, since the out-of-transit centroid offsets are unreliable if a target is saturated.

Finally, a search for close companions was performed for the remaining targets using their Gaia DR2 coordinates and the MAST (Mikulski Archive for Space Telescopes) Portal.⁴⁵ Any targets with bright ($\Delta V < 5$), close (separation $< 2''$) companions were not considered for further follow-up. Additionally, any star with a companion within $1''$ was removed, regardless of its magnitude, because it would be challenging to resolve in poorer weather conditions and could possibly contaminate flux on the slit during observations.

3.2. Spectroscopy

Once a TOI passed all photometric vetting steps, the target was queued for a reconnaissance (or recon) spectrum. A recon spectrum is an iodine-free exposure with an $S/N \approx 40 \text{ pixel}^{-1}$ to check for rapid rotation and spectroscopic false positives. Recon spectra are processed using SpecMatch (Petigura 2015) and ReaMatch (Kolbl et al. 2015).

SpecMatch estimates reliable spectroscopic stellar parameters $\{[\text{Fe}/\text{H}], T_{\text{eff}}, v \sin i, \log g\}$ from spectra with S/N

⁴³ <https://tev.mit.edu/>

⁴⁴ <https://gea.esac.esa.int/archive/>

⁴⁵ <https://mast.stsci.edu/portal/Mashup/Clients/Mast/Portal.html>

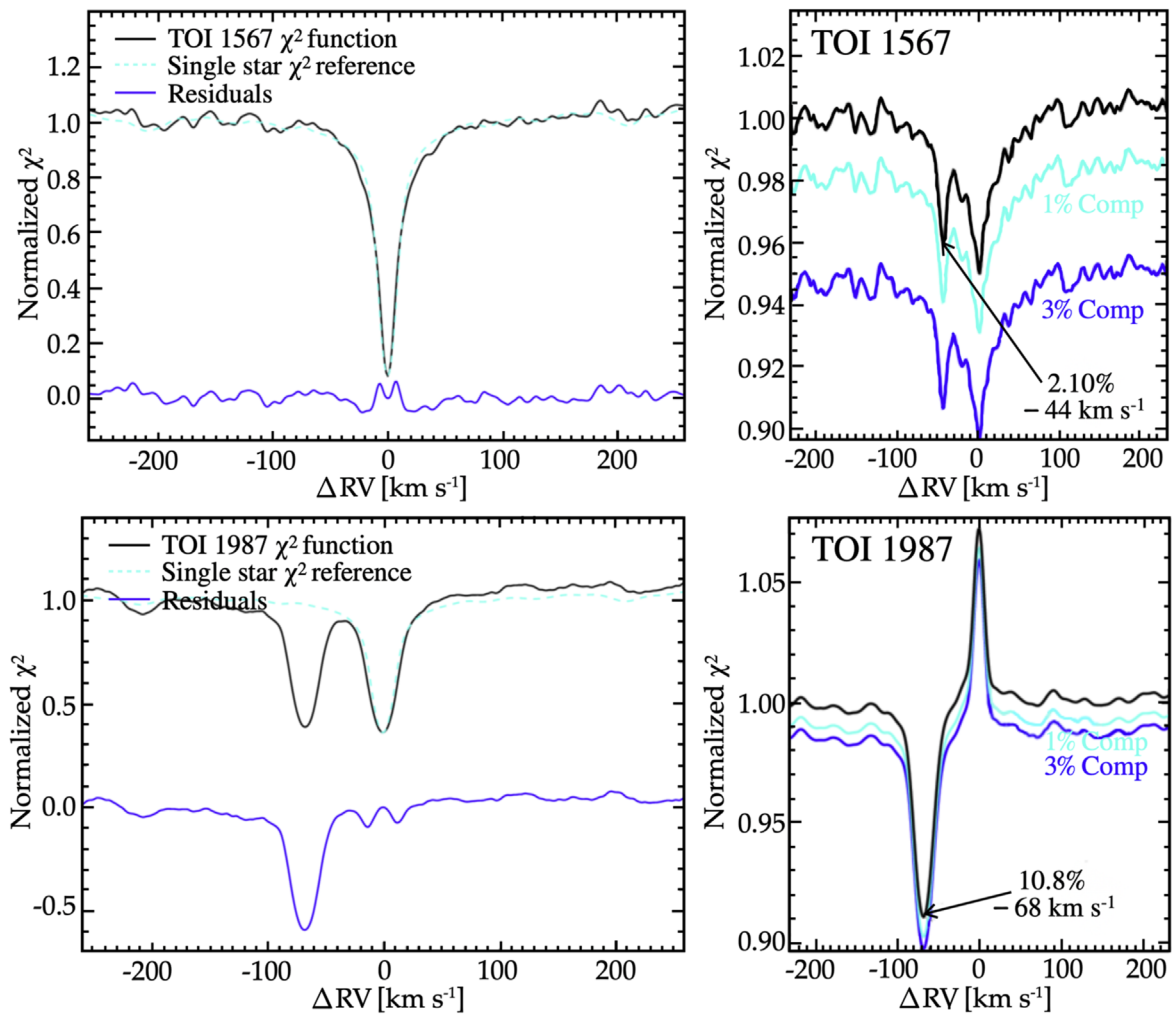


Figure 2. SB2 vetting plots for TOI 1567 and TOI 1987 from ReaMatch (Kolbl et al. 2015). Cross-correlation functions are computed from the observed spectra (left) and the residual spectra (right), after subtracting the best-fit model for the primary. Any deviations from the characteristic single-star reference suggest a stellar companion. The left panel is typically sufficient for detecting bright companions (e.g., TOI-1987), while the right panel is helpful for identifying fainter companions (e.g., TOI-1567; see Section 3.2 for more details).

$\lesssim 40/\text{pixel}$ (Petigura 2015). We used results from *SpecMatch-Syn*, which uses synthetic model atmospheres for stars with effective temperatures 4700–6500 K. *SpecMatch-Emp* (Yee et al. 2017), which relies on a comparison with empirical templates, was used for late-type stars ($T_{\text{eff}} \gtrsim 4700$ K). Smaller planet candidates orbiting stars with elevated $v \sin i$ ($\geq 8 \text{ km s}^{-1}$) were not typically considered, due to the increased number of observations required to achieve a similar mass precision (see Section 4.2 for more details).

The ReaMatch algorithm (Kolbl et al. 2015) is a spectroscopic method used to identify faint stellar companions in double-lined spectroscopic binaries (SB2). Figure 2 shows the SB2 vetting results from ReaMatch for TOIs 1567 and 1987. The left panels of Figure 2 show a cross-correlation of the observed, rest-frame corrected spectrum with an NSO Solar spectrum. Significant deviations from a single star function, as seen in the residuals, are typically sufficient for identifying brighter companions that contribute a significant fraction of flux, as seen in Figure 2 for TOI-1987.

To check for possible faint secondary lines, a best-fit spectrum is matched from the *SpecMatch* library, which is then broadened and diluted to match the absorption lines of the primary. The matched spectrum is subtracted from the observed spectrum. The

residuals are then renormalized and analyzed similarly to those of the primary. The right panels of Figure 2 show the residual cross-correlation functions (CCFs), where any large deviation from $\Delta \text{RV} \sim 0 \text{ km s}^{-1}$ is evidence for a second set of absorption lines. However, when a primary star and its stellar companion have similar radial velocities, their spectral lines will be blended, and therefore ReaMatch is limited to Doppler shifts $> 10 \text{ km s}^{-1}$.

Finally, systemic radial velocities were computed according to the methodology of Chubak et al. (2012) and compared to those from Gaia to identify single-lined spectroscopic binaries (SB1s). Targets for which the systemic and Gaia RV disagreed by more than 5 km s^{-1} typically failed this vetting step. However, for cases where systemic and Gaia RVs differed by 5 to 10 km s^{-1} , or where there was other evidence of an ambiguous false-positive detection, a second recon spectrum was taken to test for significant linear trends providing additional evidence of an SB1-like nature.

Targets that failed any of these analyses were reported to the TESS Follow-up Observing Program⁴⁶ (TFOP) Recon Spectroscopy Working Group (WG) SG2. In addition, stellar properties derived from HIRES spectra through the TK5

⁴⁶ <https://tess.mit.edu/followup/>

Table 2
TKS Spectroscopic Vetting

TIC ID	TOI	Disposition	Note
405904232	1312	SB1	
129539786	1367	...	$v \sin i = 12 \text{ km s}^{-1}$
148782377	1415	...	$v \sin i = 17 \text{ km s}^{-1}$
411608801	1494	...	$v \sin i = 15 \text{ km s}^{-1}$
376637093	1516	...	$v \sin i = 10 \text{ km s}^{-1}$
259151170	1567	SB2	
285677945	1571	...	$v \sin i = 20 \text{ km s}^{-1}$
138017750	1608	...	$v \sin i = 44 \text{ km s}^{-1}$
184679932	1645	SB1	$v \sin i = 30 \text{ km s}^{-1}$
468828873	1672	SB2	
58542531	1683	SB2	
103448870	1687	...	$v \sin i = 15 \text{ km s}^{-1}$
461662295	1711	SB1	
356978132	1755	...	$v \sin i = 11 \text{ km s}^{-1}$
450327768	1788	...	$v \sin i = 12 \text{ km s}^{-1}$
330799746	1818	SB1	$v \sin i = 10 \text{ km s}^{-1}$
20182165	1830	...	$v \sin i = 29 \text{ km s}^{-1}$
349088467	1987	SB2	$v \sin i = 110 \text{ km s}^{-1}$

Note. Spectroscopic false positives or high vsini targets that are not suitable for PRV work identified through the TESS-Keck Survey, as described in Section 3.2.^a

^a Dispositions in this table represent the false-positive classification suggested by initial TKS reconnaissance observations, and therefore do not necessarily reflect the most up-to-date TFOP dispositions.

project were/are made available to the community via the Exoplanet Follow-up Observing Program for TESS (ExoFOP-TESS) website.⁴⁷ The reported stellar parameters include spectroscopic parameters T_{eff} , $\log g$, $[\text{Fe}/\text{H}]$, and $v \sin i$, as well as stellar mass and radius derived using the spectroscopic parameters as input to `isoclassify` (Huber 2017; Berger et al. 2018). A list of spectroscopic false positives and/or stars with rapid rotation is provided in Table 2.

3.3. High-resolution Imaging

Multiplicity has historically been disfavored during follow-up target selection processes, as nearby companions can contaminate the observed spectra, resulting in less precise RVs. Similar to the Kepler efforts, the TFOP High-Resolution Imaging WG (hereafter referred to as SG3) has been reporting any stellar companions to ExoFOP TESS (e.g., Ziegler et al. 2020). For TOIs that had adaptive optics, speckle, or lucky imaging information available, we excluded TOIs for which the data or SG3 comments indicated the presence of a bright ($\Delta V < 5$ or $\Delta K < 5$) and nearby (separation $< 2''$) contaminant. For targets that had not yet been followed up by SG3, this was not a requirement for the target selection process.

There are two TOIs that failed this vetting step but made it to our final TKS target sample: TOI-1288, which only marginally failed because of the presence of two faint companions, and TOI-1443, which was added to an individual science case that did not preferentially select against binaries.

3.4. Coordination with Other Surveys

There are several ongoing, ground-based TESS RV surveys, e.g., MTS (Teske et al. 2021), NCORES (Armstrong &

consortium 2021), KESPRINT (Kabath et al. 2021), etc., many of which have science interests that overlap with those of TKS. Our target selection procedure was strategically implemented to achieve the most optimal sample that simultaneously addressed the different science goals within the survey (see Section 5 for more details). Therefore, the selection of TKS targets was independent and not influenced by selections from other surveys, which naturally led to target overlap in certain circumstances. One example is TOI 561, where both the HARPS-N and HIRES teams had a significant number of RVs and therefore coordinated paper submissions using independent analyses (Lacedelli et al. 2021; Weiss et al. 2021). For targets that were initially followed up by TKS but not part of the final selected sample, we contributed RVs to discovery papers that were typically led by non-TKS teams (e.g., TOI 442; Dreizler et al. 2020). Finally, for more uncommon situations in which there was significant target overlap, coordination often led to an exchange of RV data for multiple targets.

4. Master Target List

4.1. TOI Information

In addition to the target vetting, we constructed a master target list that provided additional information for TESS targets. The process is diagrammatically summarized in Figure 3, which also starts from a TOI release but runs in parallel to the target vetting and therefore was performed for all TOIs.

For each TOI, the TESS Input Catalogue (version 8, TICv8; Stassun et al. 2019) was queried to fetch stellar properties (e.g., radius, etc.), available photometry (i.e., Johnson V and 2-MASS JHK) and the associated Gaia Data Release 2 (DR2; Gaia Collaboration et al. 2016; Evans et al. 2018; Gaia Collaboration et al. 2018) source ID. The Gaia ID was then used to collect astrometric and photometric Gaia parameters. The TICv8 position was used with `tesspoint` (Burke et al. 2020) to determine how many sectors a given TESS target would be observed for. This was important for the TKS evolved stars (SC4) and Doppler noise (TB) aspects, both of which benefit from longer baselines. The evolutionary state of the star was calculated using `evolstate`,⁴⁸ given a star's effective temperature and radius (Huber 2017; Berger et al. 2018). For all steps that involved calculations using stellar properties, information first came from SpecMatch when a HIRES spectrum was available (see Section 3.2 for more details), otherwise the TICv8 information was used. In the event that neither were available, the stellar properties provided in the original TOI table were used.

Using the TOI planet radii, masses were computed using the following relations:

$$M_p = \begin{cases} \rho_p = 2.43 + 3.39 \left(\frac{R_p}{R_\oplus} \right) \text{ g cm}^3 & R_p < 1.5 R_\oplus \\ 2.69 \left(\frac{R_p}{R_\oplus} \right) & 1.5 R_\oplus \leq R_p < 4 R_\oplus \\ 1.24 \left(\frac{R_p}{R_\oplus} \right)^{1.7} & 4 R_\oplus \leq R_p < 11.3 R_\oplus \\ 317.83 & R_p \geq 11.3 R_\oplus. \end{cases}$$

The relations are based on Weiss & Marcy (2014) for small planets, Chen & Kipping (2017) for intermediate-mass planets,

⁴⁷ <https://exofop.ipac.caltech.edu/tess/>

⁴⁸ <https://github.com/danxhuber/evolstate/>

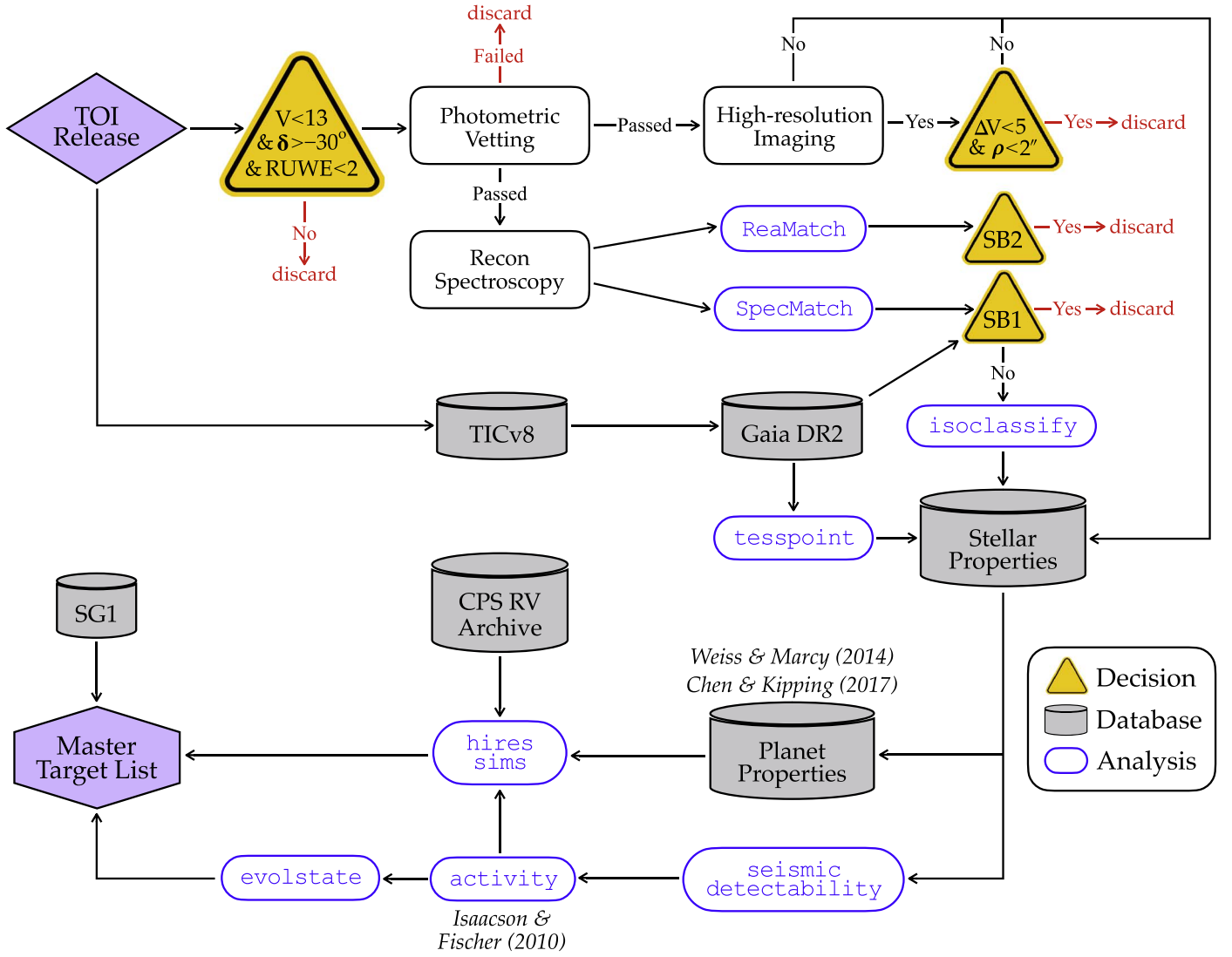


Figure 3. Flowchart summary of the TKS target vetting (Section 3) and master target list construction (Section 4) processes. Software packages are plotted in blue, while databases are shown in gray. All cuts and/or decision tree steps are in yellow, and red represents points where targets were removed from the TKS selection pool.

and assuming a Jupiter mass for planets larger than Jupiter. Expected Doppler amplitudes were calculated using

$$K_{*,\text{exp}} = \left(\frac{2\pi G}{P} \right)^{1/3} \frac{M_p}{(M_p + M_*)^{2/3}}, \quad (1)$$

where P is the orbital period, G is the gravitational constant, and M_p and M_* are the masses of the planet and star, assuming the orbit is aligned ($i = 90^\circ$) and circular ($e = 0$).

The CPS RV archive⁴⁹ was queried for targets that had existing spectra, which was important for estimating astrophysical “jitter” (Section 4.2) and expected exposure times (Section 4.3). As a final step, TOI dispositions were updated with the TESS Follow-up Observing Program (TFOP) Working Group⁵⁰ (WG) Sub Group 1 (hereafter referred to as SG1). TOIs with unfavorable or ambiguous dispositions (e.g., APC, BEB, FA, FP, NEB, etc.)⁵¹ were removed.

⁴⁹ <https://jump.caltech.edu/>

⁵⁰ <https://tess.mit.edu/followup/>

⁵¹ Ambiguous planet candidate (APC), blended eclipsing binary (BEB), false alarm (FA), false positive (FP), nearby eclipsing binary (NEB), etc.

4.2. Astrophysical Noise

To account for targets that would be challenging for PRV work, we estimated a lower limit for a single RV uncertainty by considering the contributions from various stellar sources. Specifically, we include effects from stellar rotation and magnetic activity, as well as effects due to near-surface processes like convection, granulation, and acoustic oscillations.

To estimate the Doppler noise contribution due to stellar activity (σ_{act}), we used the empirical relation from Isaacson & Fischer (2010) for stars that had the Ca II S-index and color ($B - V$) information available. For granulation and p-mode oscillations, σ_{gran} was estimated using the effective temperature and surface gravity as inputs to the RV jitter prediction code⁵² by Yu et al. (2018).

To investigate how rotation affected a typical RV observation, we calculated the median RV uncertainty for all targets from the CPS RV archive. To remove targets with observations

⁵² <https://github.com/Jieyu126/Jitter/>

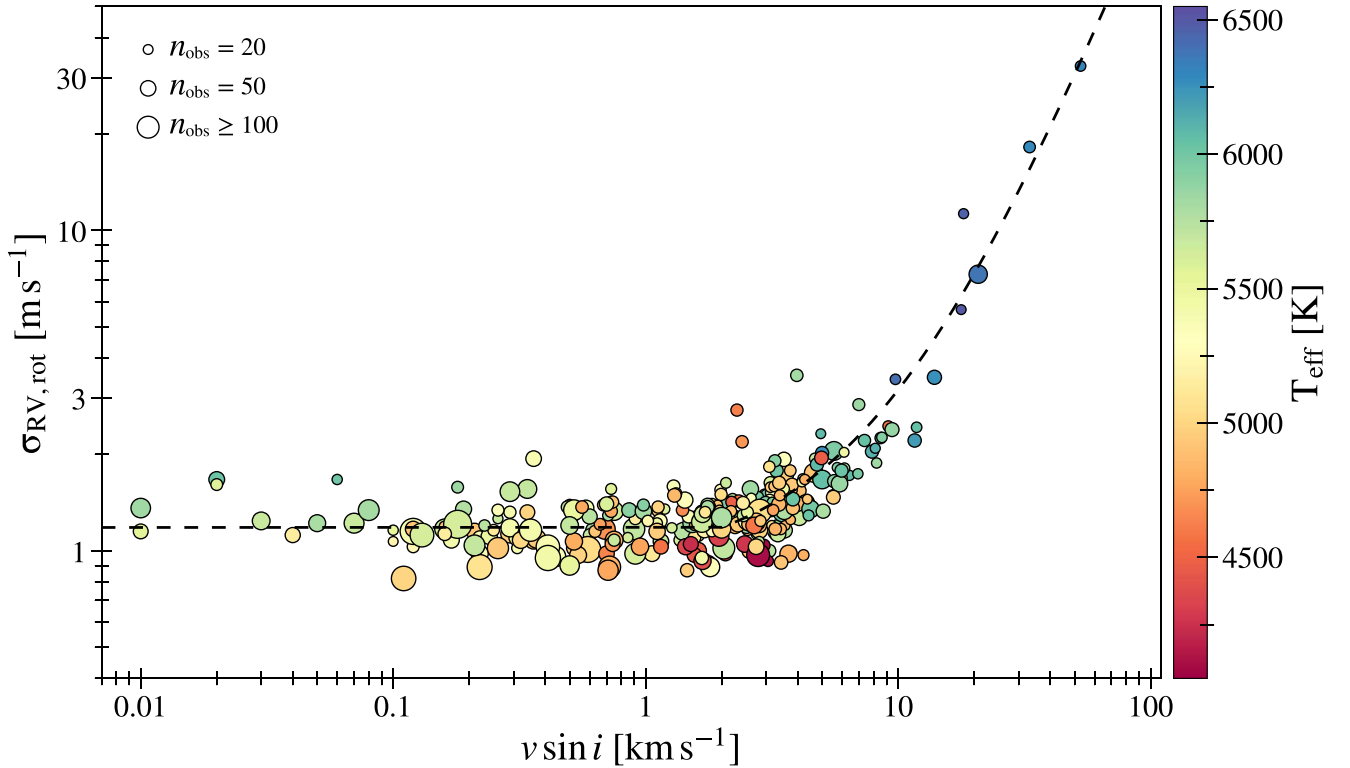


Figure 4. Median RV uncertainty vs. $v \sin i$ for all bright stars ($V < 10$) with at least 20 HRES observations and effective temperatures between 4000 K and 6500 K. Markers are sized by the number of HRES observations and colored by the effective temperature of the star. The black dashed line represents our empirical fit to the data, which is defined by the polynomial fit in Section 4.2 (Equation (2)).

that could be dominated by photon noise, we required that each star have $V < 10$. We also required that each star have an effective temperature in the range 4000–6500 K and at least 20 HRES observations. Figure 4 shows the median HRES RV uncertainty as a function of $v \sin i$. For $v \sin i < 2 \text{ km s}^{-1}$, the effects of rotational broadening are negligible and therefore the RV precision is set by the typical noise floor of the instrument and is 1.18 m s^{-1} for HRES. For moderate and high $v \sin i$ ($\geq 2 \text{ km s}^{-1}$), we fit a second-order polynomial to estimate σ_{rot} ,

$$\sigma_{\text{rot}} = 0.867 + 0.140(v \sin i) + 0.009(v \sin i)^2, \quad (2)$$

using a least-squares minimization, where σ_{rot} and $v \sin i$ are in units of m s^{-1} and km s^{-1} , respectively. The polynomial was calibrated using HRES data for stars with $v \sin i$ between $\sim 2 \text{ km s}^{-1}$ and 50 km s^{-1} .

4.3. HRES Observing Simulations

Exposure times were scaled based on the canonical exposure time of 100 s for an iodine-in observation on a $V = 8$ star in nominal conditions. For iodine-out exposures, the HRES throughput is $\sim 30\%$ higher and was therefore factored in when relevant (e.g., recon spectra, templates). The required number of counts, which determines the photon-limited RV precision (σ_{RV}), varied among science cases. A maximum exposure time of 30 minutes was implemented for all TKS observations.

The total single measurement uncertainty was then calculated using

$$\sigma_{\text{tot}}^2 = \sigma_{\text{RV}}^2 + \sigma_{\text{act}}^2 + \sigma_{\text{gran}}^2 + \sigma_{\text{rot}}^2, \quad (3)$$

which is the contribution from individual noise sources added in quadrature. The measurement uncertainty scales as

$\sigma_{\text{tot}} \propto N_{\text{obs}}^{-1/2}$, where the default number of observations for most TKS science cases was $N_{\text{obs}} = 60$. Some exceptions that warranted more observations included the multis (SC2C) and activity (TB) science cases, which instead required 100 observations. On the other hand, the distant giants (SC2A) science case preferred less precision and observations ($N_{\text{obs}} = 15$) in exchange for more targets and longer baselines.

An average overhead of 120 s was charged per target per observation, to account for telescope slew time and CCD readout times. For science cases that depended on a certain mass precision (e.g., SC3), total nominal exposure times to achieve 5σ ($t_{5\sigma, \text{HRES}}$) and 10σ ($t_{10\sigma, \text{HRES}}$) masses were calculated for all TOIs. Finally, to estimate realistic target costs, calculations also included archival HRES data and factored in the availability of high-resolution templates.

4.4. Individual Science Case Selection Criteria

4.4.1. SC1A: Planet Radius Gap

The focus of SC1A is bulk properties of planets in the radius valley. However, to increase overlap with other science cases, the radius limits were expanded to include any planets in the range of $1 R_{\oplus} < R_p < 3.5 R_{\oplus}$.

4.4.2. SC1B: Stellar Flux and Gaseous Envelopes

SC1B focuses on a narrow range of planet sizes that are exposed to very different stellar environments, in particular, on smaller planets with sizes $1 R_{\oplus} < R_p < 4 R_{\oplus}$ and with orbital periods up to 100 days. To avoid sample biases, targets in this parameter space were selected as uniformly and as randomly as possible. To achieve this, 12 bins were created in roughly equal

bin sizes in two-dimensional log-linear space, with planet radius bin edges of $R_p \sim [1, 2, 3, 4] R_\oplus$ (i.e., linear-space) and orbital period bin edges of $P \sim [1, 3, 10, 30, 100]$ days (i.e., log-space).

4.4.3. SC1C: Ultra-short-period Planets

SC1C is primarily interested in differentiating between the smaller ($< 2 R_\oplus$) USP population that appear to have \sim Earth-like compositions and the recently discovered sub-day hot Neptunes (e.g., TOI-849 b; Armstrong et al. 2020). Therefore, the selection criteria for SC1C includes both classes of sub-Jovian planets, with $R_p < 8 R_\oplus$ and $S_{\text{inc}} > 650 S_\oplus$.

4.4.4. SC1D: Habitable Zone Planets

We selected potential habitable zone planets based on their incident flux. We adopted a limit of $< 10 S_\oplus$ and required all SC1D targets to orbit main-sequence stars.

4.4.5. SC1E: Planet-Star Correlations

To enable statistical investigations of possible correlations between stellar and planetary properties, we selected planets orbiting stars with a wide range of masses and metallicities. In order to ensure that low-mass stars were observed despite their faintness, TOI-1467 and TOI-1801 were added manually as high-priority targets (see Section 6). Due to the broad parameter space covered by this science case, almost all selected targets had overlap with multiple science cases.

4.4.6. SC2A: Distant Giants

We selected all main-sequence stars brighter than $V = 12$ that have an approximately solar-like mass ($0.5 M_\odot \leq M_* \leq 1.5 M_\odot$). We avoided rapidly rotating and/or active stars by also applying cuts in T_{eff} (≤ 6200 K \approx Kraft Break) and $\log R'_{HK}$ (≤ -4.7). For stars that had recon spectra available and thus a measured projected velocity, we excluded anything with a $v \sin i \geq 5 \text{ km s}^{-1}$. We also excluded stars with Gaia RUWE > 1.3 .

We only selected targets with multiple event statistics (MES) of at least 12, which indicate high-quality transit detections based on a visual inspection of SPOC DV reports. Only systems that contained at least one transiting planet smaller than $10 R_\oplus$ were kept (J. Van Zandt et al. 2022, in preparation).

4.4.7. SC2B: Obliquities and Eccentricities

Obliquity targets were selected on a case-by-case basis. To select high-probability eccentric planet candidates, we performed transit fitting of the PDCSAP light curves (Smith et al. 2012; Stumpe et al. 2012, 2014) to measure the photoeccentric effect, which compares the observed transit duration with the expected duration for a circular orbit (Dawson & Johnson 2012; Kipping et al. 2012). Transit duration is related to the eccentricity (e) and the argument of periastron (ω) by

$$T_{14} = \left(\frac{R_* P}{\pi a} \sqrt{1 - b^2} \right) \frac{\sqrt{1 - e^2}}{1 + e \sin \omega}, \quad (4)$$

where T_{14} is the total transit duration (i.e., from first to final contact), R_* is the stellar radius, P is the orbital period, b is the impact parameter, and a is the planet's semimajor axis (Winn 2010).

Instead of using the standard transit parameter a/R_* , we reparameterized our model in terms of stellar density (ρ_*), which maps to a/R_* through Kepler's Third Law and can be measured independently. We combined this with Equation (4), which yielded a new parameter ($\rho_{*,\text{circ}}$) that was directly sampled in our transit modeling using `exoplanet` (Foreman-Mackey 2019). We derived an eccentricity estimate by resampling from the posterior distribution of $\rho_{*,\text{circ}}$ and comparing these values to an independent stellar density measurement derived by combining HIRES spectroscopy, Gaia parallaxes, and isochrone models. We selected all targets for which zero eccentricity is ruled out at the 2σ level via this method (M. G. MacDougall et al. 2022, in preparation).

4.4.8. SC2C: Multis

The only selection requirement for SC2C was the presence of more than one transiting planet. Systems with the highest planet multiplicity were ranked the highest. For systems with the same number of planet candidates, priority was given to lower-cost targets (i.e., brighter and/or shared targets).

4.4.9. SC3: Atmospheres

The Transmission Spectroscopy Metric (TSM) from Kempton et al. (2018) is an S/N proxy for atmospheric observations and was computed for all planet candidates. The TSM is defined as:

$$\text{TSM}_p = S \times \frac{R_p^3 T_{\text{eq}}}{M_p R_*^2} \times 10^{-0.2 m_J}, \quad (5)$$

where S is a dimensionless normalization constant,

$$S = \begin{cases} 0.19, & R_p < 1.5 R_\oplus \\ 1.26, & 1.5 < R_p < 2.75 R_\oplus \\ 1.28, & 2.75 < R_p < 4.0 R_\oplus \\ 1.15, & 4.0 < R_p < 10 R_\oplus. \end{cases}$$

Quantitatively, the TSM is the expected (or simulated) S/N from a 10 hr observation with JWST-NIRISS, assuming a cloud-free, solar-metallicity, H_2 -dominated atmosphere. For reference, a “good” TSM for a sub-Neptune ($1.5 < R_p < 4.0 R_\oplus$) is roughly between 80 and 150 (see Table 1 in Kempton et al. 2018). In the end, the metric used by SC3 was the ratio of the TSM to the total expected Keck/HIRES time to obtain a 5σ mass ($t_{5\sigma, \text{HIRES}}$) as a way to penalize highly ranked targets that would require a disproportionate amount of telescope resources.

In order to select optimal targets across a broad range of parameters, SPOC-identified (Jenkins et al. 2016) TOIs were divided into log-uniform bins by their planet radius (R_p), stellar effective temperature (T_{eff}), and incident flux (S_{inc}). For posterity, bin edges were located at $R_p \sim [1.0, 1.6, 2.5, 4.0, 6.3, 11.2] R_\oplus$, $T_{\text{eff}} \sim [2500, 3900, 5200, 6500]$ K, and $S_{\text{inc}} \sim [10^{-1}, 10^0, 10^1, 10^2, 10^3, 10^4] S_\oplus$. Confirmed planets were added to these bins in order to highlight interesting outliers and more easily identify TOIs that would sample a new region of parameter space. All candidates in a given bin were then ranked by the metric discussed above (i.e., $\text{TSM}/t_{5\sigma, \text{HIRES}}$), where careful consideration was given to the five highest-ranked candidates in each bin. Ultimately, a subset of these targets were hand-selected on an individual basis and

identified as high-priority targets for SC3 (i.e., denoted as 3[†] in Table 3).

4.4.10. SC4: Evolved

To identify higher-priority targets that were likely to exhibit solar-like oscillations, asteroseismic detection probabilities were computed for all TOIs (Chaplin et al. 2011; Schofield et al. 2019). Broadly speaking, asteroseismic detection probabilities increase with luminosity and longer time series. Schofield et al. (2019) calculated probabilities for the TIC prior to the TESS launch, which required assumptions about the number of sectors of TESS observations for each potential target. Consequently, we recalculated detection probabilities using the actual number of sectors. The selection criteria for SC4 required either an evolved star status (subgiant or red giant) for new planet candidate hosts or a predicted asteroseismic detection probability ≥ 0.5 .

4.4.11. TB: Astrophysical Doppler Noise

For stars that had HIRES spectra available, an activity metric was computed for the Doppler noise aspect using traditional activity indicators for chromospheric emission like $\log R'_{HK}$ and the estimated jitter. Targets with known rotation periods and longer baselines were typically given higher priorities. Gaussian weights centered on $\log R'_{HK} = -4.8$ ensured a moderate level of activity while downweighting both inactive stars, which would not be as scientifically interesting, as well as very active stars that would be challenging to characterize. Using the σ_{tot} metric calculated in Equation (3) (Section 4.2), Gaussian weights were centered on a “jitter” value of 4 m s^{-1} based on a rationale similar to that used for the chromospheric emission. Finally, brighter stars were ranked in ascending order, which was helpful for narrowing the targets down by an order of magnitude. However, more active targets require multiple considerations, and therefore the final high-priority high-cadence targets were hand-selected for this case.

5. Automated Target Selection

5.1. Motivation and Initial Conditions

Using the master target list described in Section 4, the goal was to develop an automated and reproducible procedure to select targets given a set of science cases and time allocation. Specifically, a set of programs, $P \supset \{P_1, P_2, \dots, P_n\}$ receive time allocations $T \sim \{T_1, T_2, \dots, T_n\}$ of the total observing time allocation, T_{tot} . A set of stars, $S \supset \{S_1, S_2, \dots, S_m\}$ have a set of observing times per star, $t \sim \{t_1, t_2, \dots, t_m\}$, which can vary for each program. Each program has a set of ordinal rankings, $R \sim \{R_1, R_2, \dots, R_m\}$ for the set of stars S . In addition, some programs may want to update their rankings after each selection step, and therefore individual program rankings have the flexibility to adapt and update with each iteration. This encourages cooperation because a program would rank a shared star more highly, which would ultimately cost that program (and other programs) less.

A key component of the target selection algorithm is the `Survey` class, which includes general survey information, science-case-specific requirements, and the vetted planet sample. Individual programs are able to specify an observing strategy (i.e., the total number of observations and required photon counts), any high-priority or dropped targets, as well as

the selection criteria to filter a program by. Upon the initialization of the `Survey` class, an initial accounting of the vetted sample occurs by determining the number of relevant science targets (or “picks”) available for each program in the `Survey`. This is a required check to make sure that, at any point during the target selection process, the number of program picks does not exceed the available number of targets for a given science case.

Each program within the `Survey` can specify how to prioritize and select their targets. Additionally, programs are not limited to a single criterion but instead can rank targets by providing a list of prioritization metrics. An example is SC2C, whose targets were first ranked by those with the highest planet multiplicity and then by target cost. For atmospheric targets, TOIs were prioritized by the TSM metric discussed in Section 4.4.9 and then sorted by cost. However, for situations that involved more complicated vetting (e.g., SC2A) or meticulous observing plans (e.g., SC2Bii) whose prioritization could not be automated, a list of rankings could be provided that did not change under any circumstances. This was particularly important for a majority of SC2 that focused on dynamical planets, which provided an outlet for target lists to “override” any automated process.

5.2. Algorithm

A data-flow diagram of the target prioritization algorithm is shown in Figure 5. In summary, the following steps occur while the total remaining time, $T_{\text{tot}} \equiv \sum_n T_n$ for n science cases in a `Survey` is greater than zero:

1. A program is selected at random, with a probability of selection that is proportional to the fractional amount of time remaining for each science case in the `Survey`. Specifically, the program calculates the cumulative distribution function by normalizing the most current list of remaining times for n science cases by T_{tot} . Therefore, a uniform random number on the unit interval $\sim [0, 1]$ will accurately map back to the n discrete science cases and select a program from the `Survey`.
2. The vetted `Survey` sample (see Section 3) is filtered based on the selected program’s selection criteria (see Section 4.4) to include only the relevant science targets. This is done by initializing a `Sample` class object, which updates the target `Sample` costs based on past algorithm selections. After cost updates are calculated, targets are ranked based on the prioritization metric(s) of the selected program. If the program provided any high-priority targets, all priority targets would be ranked first, followed by regular-priority targets that are assigned rankings.
3. The selected program chooses the highest-ranked star that has not yet been selected by that program.
 - (a) If the selected program *can* afford the target (i.e., has the available time), the program is charged the required observing time for the selected star and the target is appended to the final `Survey` target list. If the target has already been selected by other programs in previous iterations, relevant programs are credited back any differences in costs.
 - (b) If the selected program *cannot* afford the target (i.e., the required time for the highest ranked target exceeds the remaining time available for the program), the

Table 3
TKS Target Sample

TOI	TIC	R.A. (deg)	δ (deg)	V (mag)	T_{eff} (K)	R_p (R_{\oplus})	Period (days)	S_{inc} (S_{\oplus})	Science Cases ^a
260.01	37749396	4.7732	-9.9648	9.90	4049	1.64	13.47	1.1e+01	1A, 1B, TA, TB ^b
266.01	164767175	26.2096	-18.4009	10.07	5784	2.41	10.77	1.0e+02	1A, 1B, 3 ^b , TA, TB
266.02	1.76	6.19	2.2e+02	1A, 1B, 3, TA, TB
329.01	169765334	351.3209	-15.6347	11.26	5560	10.84	5.70	3.6e+03	4, TA, TB
465.01	270380593	32.7818	+2.4180	11.56	4936	5.64	3.84	1.5e+02	2A, TA, TB
469.01	33692729	93.0582	-14.6500	9.49	5283	3.69	13.63	8.9e+01	1B, 3 ^b , TA, TB
480.01	317548889	88.3787	-16.2650	7.28	6212	3.08	6.87	3.7e+02	1A, 1B, 4 ^b , TA, TB
509.01	453211454	117.9250	+9.3861	8.58	5560	3.07	18.12	4.6e+01	1A, 1B, 2A, 3 ^b , TA, TB
554.01	407966340	60.7479	+9.2085	6.91	6337	3.41	7.05	4.2e+02	1A, 1B, 3 ^b , TA, TB
561.01	377064495	148.1856	+6.2164	10.25	5440	3.77	10.78	6.6e+01	1A, 1B, 1C, 2C, 3, TA, TB
561.02	1.55	0.45	4.6e+03	1A, 1B, 1C, 2C, 3 ^b , TA, TB
561.03	2.84	16.37	3.8e+01	1A, 1B, 1C, 2C, 3, TA, TB
669.01	124573851	158.9006	-5.1817	10.61	5624	3.84	3.95	6.4e+02	1B, 3 ^b , TA, TB
1136.01	142276270	192.1849	+64.8553	9.53	5767	4.72	12.52	7.7e+01	1A, 1B, 2C, 3, TA, TB ^b
1136.02	3.00	6.26	2.1e+02	1A, 1B, 2C, 3, TA, TB ^b
1136.03	4.04	26.32	3.0e+01	1A, 1B, 2C, 3 ^b , TA, TB ^b
1136.04	2.54	18.80	4.8e+01	1A, 1B, 2C, 3, TA, TB ^b
1173.01	232967440	197.6823	+70.7684	11.04	5322	9.22	7.06	8.1e+01	2A, TA, TB
1174.01	154089169	209.2181	+68.6180	10.96	5077	2.31	8.95	4.4e+01	2A, TA, TB
1180.01	158002130	214.5531	+82.1940	11.02	4700	2.85	9.69	3.5e+01	2A, TA, TB
1181.01	229510866	297.2159	+64.3544	10.58	6122	16.66	2.10	4.0e+03	4, TA, TB
1184.01	233087860	272.2039	+60.6782	10.99	4534	2.40	5.75	5.3e+01	2Bi ^b , TA, TB
1194.01	147950620	167.8205	+69.9647	11.30	5323	8.86	2.31	6.4e+02	2A, TA, TB
1244.01	219850915	256.2803	+69.5194	11.93	4599	2.39	6.40	5.6e+01	2A, TA, TB
1246.01	230127302	251.1165	+70.4296	11.63	5141	3.33	18.65	2.7e+01	2A, 2C, TA, TB
1246.02	3.00	4.31	2.0e+02	2A, 2C, TA, TB
1246.03	2.63	5.90	1.3e+02	2A, 2C, TA, TB
1246.04	3.26	37.92	1.0e+01	2A, 2C, TA, TB
1247.01	232540264	227.8705	+71.8410	9.08	5711	2.80	15.92	7.0e+01	1A, 1B, 2A, 3 ^b , TA, TB ^b
1248.01	232612416	259.0236	+63.1060	11.81	5227	6.62	4.36	2.0e+02	2A, TA, TB
1249.01	232976128	200.5617	+66.3087	11.09	5453	3.15	13.08	3.1e+01	2A, TA, TB
1255.01	237222864	296.2443	+74.0627	9.92	5126	2.70	10.29	5.9e+01	1A, 1B, 2A, 2Bi ^b , 3, TA, TB
1269.01	198241702	249.6971	+64.5587	11.62	5517	2.38	4.25	2.3e+02	2A, TA, TB
1269.02	2.32	9.24	8.2e+01	2A, TA, TB
1272.01	417948359	199.1966	+49.8610	11.76	4987	4.29	3.32	2.2e+02	2A, 2Bi ^b , 3, TA, TB
1279.01	224297258	185.0639	+56.2011	10.71	5477	2.58	9.62	1.0e+02	2A, TA, TB
1288.01	365733349	313.1666	+65.6091	10.45	6180	4.73	2.70	6.9e+02	2A, TA, TB
1294.01	219015370	223.0929	+70.4766	11.31	5714	9.30	3.92	3.2e+02	4, TA, TB
1296.01	219854185	256.7709	+70.2385	11.37	5494	14.86	3.94	8.4e+02	4, TA, TB
1298.01	237104103	241.3234	+70.1899	11.89	5731	10.15	4.54	5.1e+02	4, TA, TB
1339.01	269701147	302.0240	+66.8506	8.97	5461	3.20	8.88	9.9e+01	1A, 1B, 2A, 2C, 3 ^b , TA, TB
1339.02	3.07	28.58	2.0e+01	1A, 1B, 2A, 2C, 3, TA, TB
1339.03	1.74	...	2.5e+01	1A, 1B, 2A, 2C, 3, TA, TB
1347.01	229747848	280.3268	+70.2899	11.17	5424	2.06	0.85	1.9e+03	1A ^b , 1B, 1C, 2Bi ^b , TA, TB
1347.02	1.78	4.84	1.8e+02	1A ^b , 1B, 1C, 2Bi, TA, TB
1386.01	343019899	334.5037	+54.3190	10.61	5769	6.55	...	-1.0e+00	2Bi ^b , TA, TB
1410.01	199444169	334.8832	+42.5603	11.11	4507	2.94	1.22	5.6e+02	1A, 1B, 2A, 3 ^b , TA, TB
1411.01	116483514	232.9451	+47.0568	10.51	4184	1.37	1.45	2.8e+02	2A, TA, TB
1422.01	333473672	354.2412	+39.6394	10.62	5914	3.09	13.00	8.7e+01	2A, TA, TB
1430.01	293954617	300.6143	+53.3768	9.19	5064	2.23	7.43	7.2e+01	1A, 1B, 3 ^b , TA, TB
1436.01	154383539	215.6025	+55.3337	12.01	5011	1.72	0.87	1.1e+03	1C ^b , 1E ^b , TA, TB ^b
1437.01	198356533	256.1387	+56.8426	9.17	6093	2.35	18.84	8.7e+01	1A, 1B, 2A, TA, TB
1438.01	229650439	280.9243	+74.9376	10.96	5259	2.81	5.14	1.2e+01	2A, TA, TB
1438.02	2.32	9.43	6.4e+01	2A, TA, TB
1439.01	232982558	241.7639	+67.8777	10.55	5873	3.43	27.64	3.9e+01	4, TA, TB
1443.01	237232044	297.4003	+76.1391	10.68	5236	2.07	23.54	1.5e+01	2A, TA, TB
1444.01	258514800	305.4743	+70.9438	10.94	5466	1.29	0.47	5.0e+03	1C ^b , 2A, TA, TB
1451.01	417931607	186.5243	+61.2590	9.58	5781	2.46	16.54	2.6e+01	1A, 1B, 2A, TA, TB
1456.01	199376584	306.7413	+33.7445	8.56	6125	7.70	12.16	2.2e+02	3, TA, TB
1467.01	240968774	19.1139	+49.2338	12.29	3834	1.83	5.97	1.8e+01	1E ^b , TA, TB
1471.01	306263608	30.9043	+21.2809	9.20	5625	4.28	20.77	8.1e+01	2A, 3 ^b , TA, TB
1472.01	306955329	14.1136	+48.6376	11.30	5103	4.31	6.36	1.1e+02	2A, TA, TB
1473.01	352413427	15.5982	+37.1855	8.84	5958	2.49	5.26	3.0e+02	1A, 1B, 3 ^b , TA, TB ^b

Table 3
(Continued)

TOI	TIC	R.A. (deg)	δ (deg)	V (mag)	T_{eff} (K)	R_p (R_{\oplus})	Period (days)	S_{inc} (S_{\oplus})	Science Cases ^a
1601.01	139375960	38.3614	+41.0134	10.66	5917	14.61	5.33	1.1e+03	4, TA, TB
1611.01	264678534	325.1866	+84.3335	8.37	5071	2.72	16.19	6.6e+01	1A, 1B, 2A, TA, TB
1669.01	428679607	45.9529	+83.5876	10.22	5550	2.25	2.68	6.9e+02	2A, TA, TB
1691.01	268334473	272.4061	+86.8596	10.13	5759	3.75	16.73	5.9e+01	2A, TA, TB
1694.01	396740648	97.7482	+66.3607	11.45	5058	5.48	3.77	2.0e+02	2A, TA, TB
1710.01	445805961	94.2828	+76.2108	9.54	5675	5.41	24.28	3.5e+01	2A, TA, TB
1716.01	14336130	105.0829	+56.8244	9.41	5878	2.74	8.09	2.5e+02	1A, 1B, 2A, TA, TB
1723.01	71431780	116.7971	+68.4766	9.66	5777	3.16	13.72	9.1e+01	2A, TA, TB
1726.01	130181866	117.4794	+27.3632	6.92	5694	2.16	7.11	1.4e+02	1A, 1B, TA, TB ^b
1726.02	2.64	20.55	3.5e+01	1A, 1B, 2Bii ^b , TA, TB ^b
1736.01	408618999	43.4350	+69.1014	8.95	5656	2.74	7.07	2.0e+02	1A, 1B, 3 ^b , 4, TA, TB
1742.01	219857012	257.3285	+71.8764	8.86	5707	2.20	21.27	5.5e+01	1A, 1B, 2A, TA, TB
1751.01	287080092	243.4888	+63.5343	9.33	6114	2.81	37.47	3.8e+01	1A, 1B, 2A, TA, TB
1753.01	289580577	252.4698	+61.1735	11.83	5700	2.96	5.38	2.4e+02	2A, TA, TB
1758.01	367858035	354.7430	+75.6851	10.79	5169	3.80	20.70	2.0e+01	2A, TA, TB
1759.01	408636441	326.8533	+62.7539	11.93	3960	3.23	37.70	2.0e+00	1D ^b , 2A, 3 ^b , TA, TB
1775.01	9348006	150.1151	+39.4578	11.65	5251	8.07	10.24	6.0e+01	2A, TA, TB
1776.01	21535395	164.7761	+40.9836	8.26	5723	1.40	2.80	5.6e+02	1A, 1B, 3, TA, TB
1778.01	39699648	136.7781	+46.6726	8.99	6023	2.83	6.52	4.1e+02	1A, 1B, TA, TB
1794.01	286916251	203.3977	+49.0611	10.32	5707	3.03	8.77	2.0e+02	2A, TA, TB
1797.01	368435330	162.7771	+25.6412	9.18	5922	3.21	3.65	5.4e+02	1A, 1B, 2A, TA, TB
1798.01	198153540	211.0941	+46.5194	11.36	5165	2.39	8.02	6.9e+01	1C ^b , TA, TB
1798.02	1.28	0.44	3.4e+03	1C, TA, TB
1799.01	8967242	167.2330	+34.3032	8.98	5690	1.63	7.09	1.6e+02	1A, 1B, TA, TB
1801.01	119584412	175.5766	+23.0269	11.58	3815	2.17	21.28	3.0e+00	1D ^b , 1E ^b , TA, TB
1807.01	180695581	201.2833	+38.9225	10.00	4612	1.53	0.55	1.6e+03	1A, 1C, TA, TB ^b
1823.01	142381532	196.2204	+63.7538	10.73	4760	8.14	194.05	9.0e+00	2A, TA, TB
1824.01	142387023	197.7312	+61.7448	9.72	5182	2.40	22.81	1.7e+01	1A, 1B, 2A, TA, TB ^b
1836.01	207468071	245.9082	+54.6898	9.77	6351	7.88	20.38	1.1e+02	4, TA, TB
1842.01	404505029	201.9628	+9.0307	9.81	6115	12.68	19.15	2.4e+02	4, TA, TB
1898.01	91987762	144.5556	+23.5469	7.87	6303	7.16	...	2.0e+02	4, TA, TB
1905.01	429302040	188.3869	-10.1461	11.59	4251	12.84	5.72	3.7e+01	2Bii, TA, TB
2019.01	159781361	234.4317	+48.9554	10.26	5588	6.09	15.35	1.9e+02	4, TA, TB
2045.01	347013211	1.1191	+54.9345	11.30	6125	12.97	9.08	5.4e+02	4, TA, TB
2076.01	27491137	217.3927	+39.7904	9.14	5163	2.89	10.36	4.8e+01	1A, 1B, 1D ^b , TA, TB
2076.02	4.30	33.69	9.0e+00	1A, 1B, 1D ^b , TA, TB
2088.01	441765914	261.3752	+75.8823	11.64	4902	3.51	124.73	1.0e+00	1D ^b , 1E ^b , 3, TA, TB
2114.01	9828416	261.0964	+33.2051	10.27	6382	13.87	6.21	5.3e+02	4, TA, TB
2128.01	21832928	256.9826	+32.1055	7.22	5991	1.97	16.33	8.6e+01	1A, 1B, TA, TB
2145.01	88992642	263.7581	+40.6951	9.07	6202	12.41	10.26	1.1e+03	4, TA, TB

Notes. Values in this table represent those used during the target selection and therefore do not necessarily reflect the most up-to-date values. Duplicated target information for TOIs with more than one transiting planet candidate have been omitted.

^a Please refer to Table 1 for the definition of science case keys.

^b High-priority targets provided during the target selection process, as indicated by the individual program.

program is temporarily stuck. The “stuck” feature enabled the continuation of the algorithm by allowing a program to pass without removing it from the selection process altogether. The main reason for this is that as the algorithm progresses, including more target selections, a given target might suddenly become affordable if it is shared by enough programs.

The above steps repeat until either (1) all resources have been exhausted (i.e., $T_{\text{tot}}=0$) or (2) all programs in the Survey are “stuck.” Once one of these conditions is satisfied, the selection process is complete and the program will save a number of data products. The data products include a csv file with the target list and the Track, which records the detailed history (i.e., every iteration) of the selection process. Finally, an additional Monte Carlo-like simulation is an available option

to test how robust (or sensitive) the sample is due to the inherent randomness of the selection process, which is achieved by running the algorithm multiple times and using the static list of seeds to set the random number generator (i.e., reproducible).

6. TKS Target Sample

For TKS allocations, most science cases started with an equal amount of time (10% of T_{tot}), with the exception of SC1D, which started with half of that allocation (5% of T_{tot}). In addition, 10% of T_{tot} was designated to TB for high-cadence, high-priority activity targets, while TA did not require any allocation. Figure 6 shows the complete TKS sample (orange) selected by the prioritization algorithm using an allocation of 50 nights and assuming 10 hr per night. Almost all of the

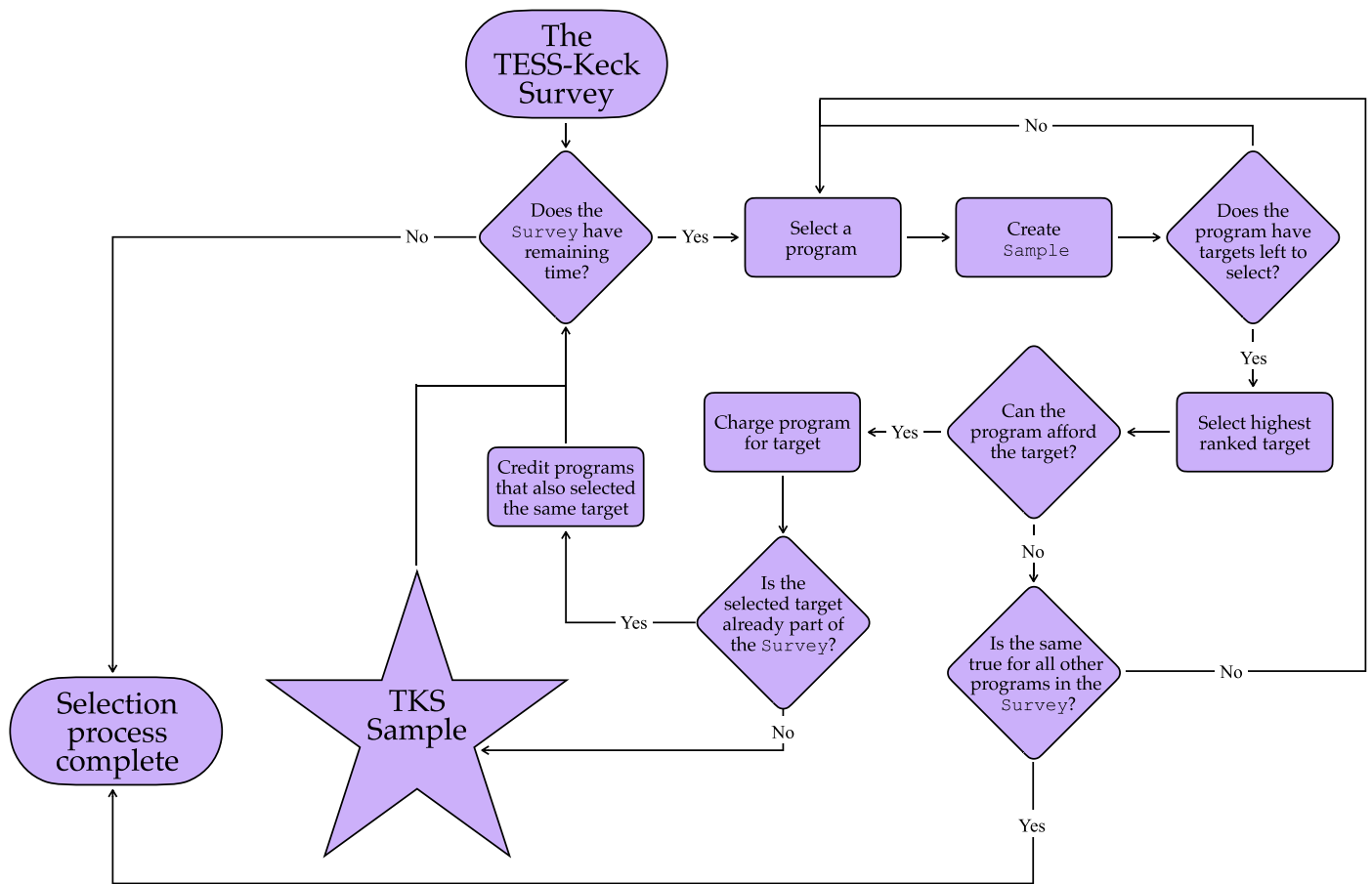


Figure 5. Flow diagram for the survey target prioritization algorithm. The `Survey` class contains all programmatic survey information as well as the vetted sample. The selection process will continue until either all of the time in the `Survey` is used or all science cases in the `Survey` are no longer able to make selections.

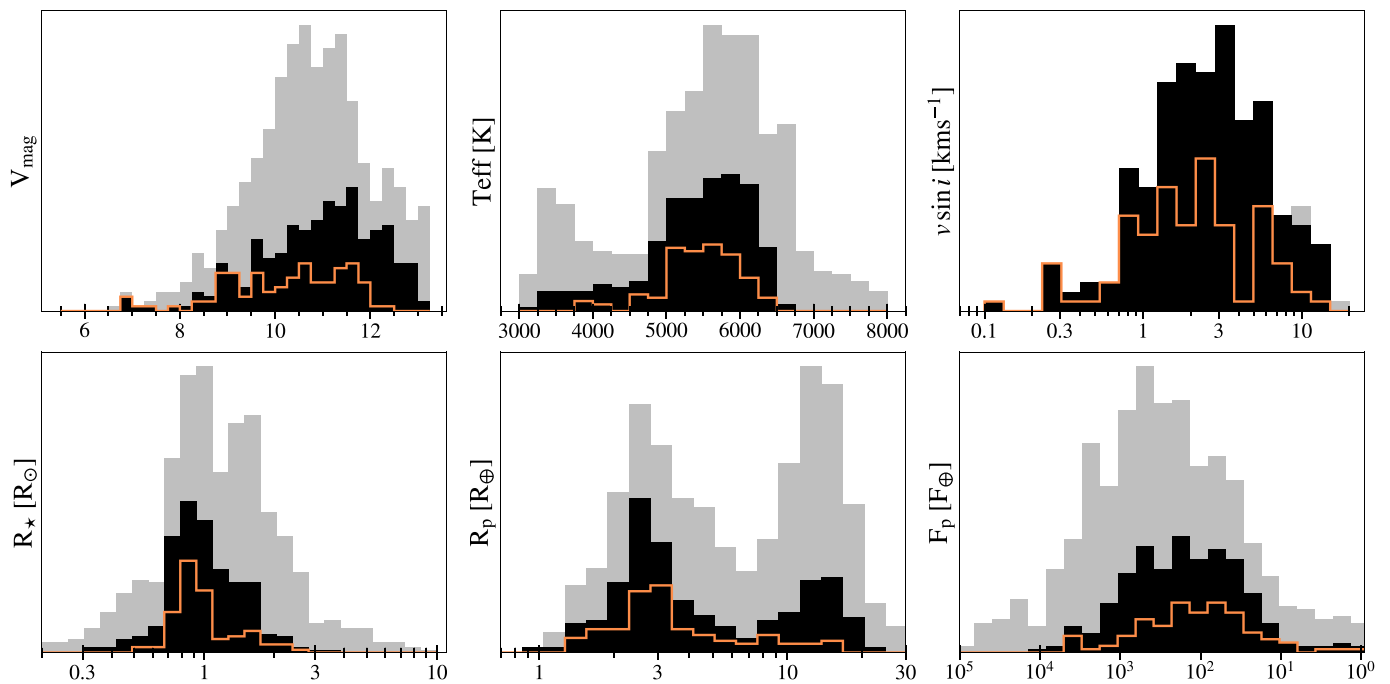


Figure 6. All TESS Objects of Interest above a decl. of $\delta > -30^\circ$ with a low Gaia RUWE < 2 (gray sample). The black sample comprises all TOIs that passed every vetting step and therefore were available for target selection. The final TKS sample that was selected by the target prioritization algorithm is shown by the orange line.

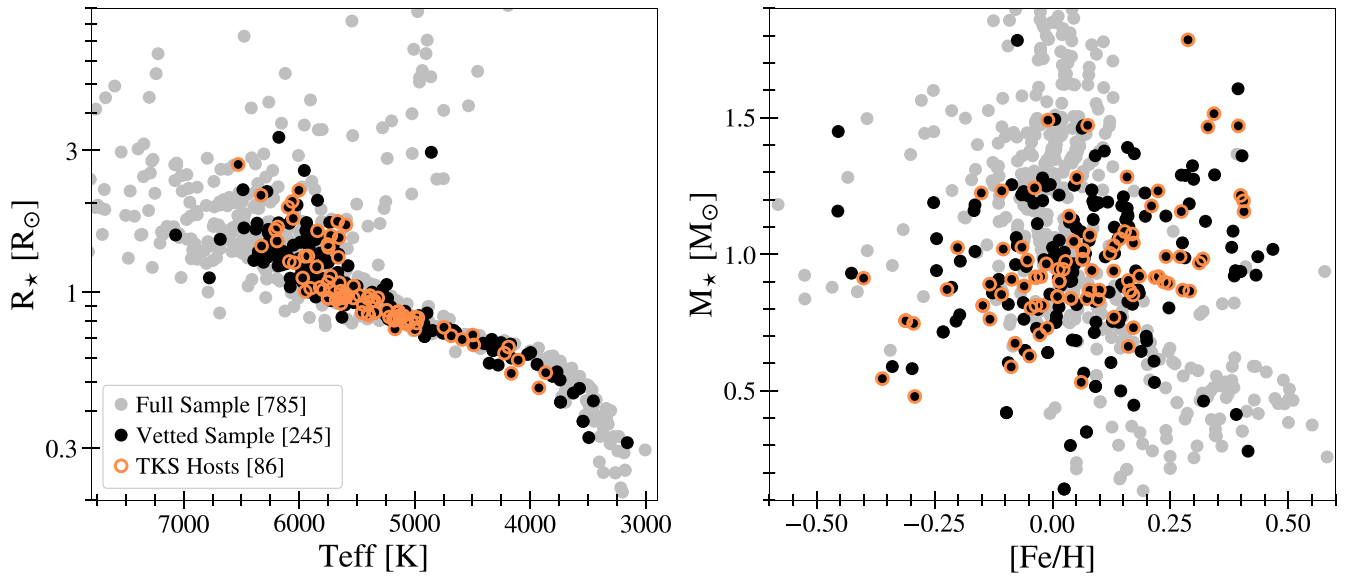


Figure 7. TESS Objects of Interest plotted in an HR-diagram (left) and in stellar mass–metallicity space (right). Gray symbols represent all TOIs with $\delta > = -30^\circ$ and Gaia RUWE metric < 2 . Black symbols represent TOI hosts that passed all vetting steps and were thus available during the target selection process, while the final TKS sample selected by the algorithm is shown in orange.

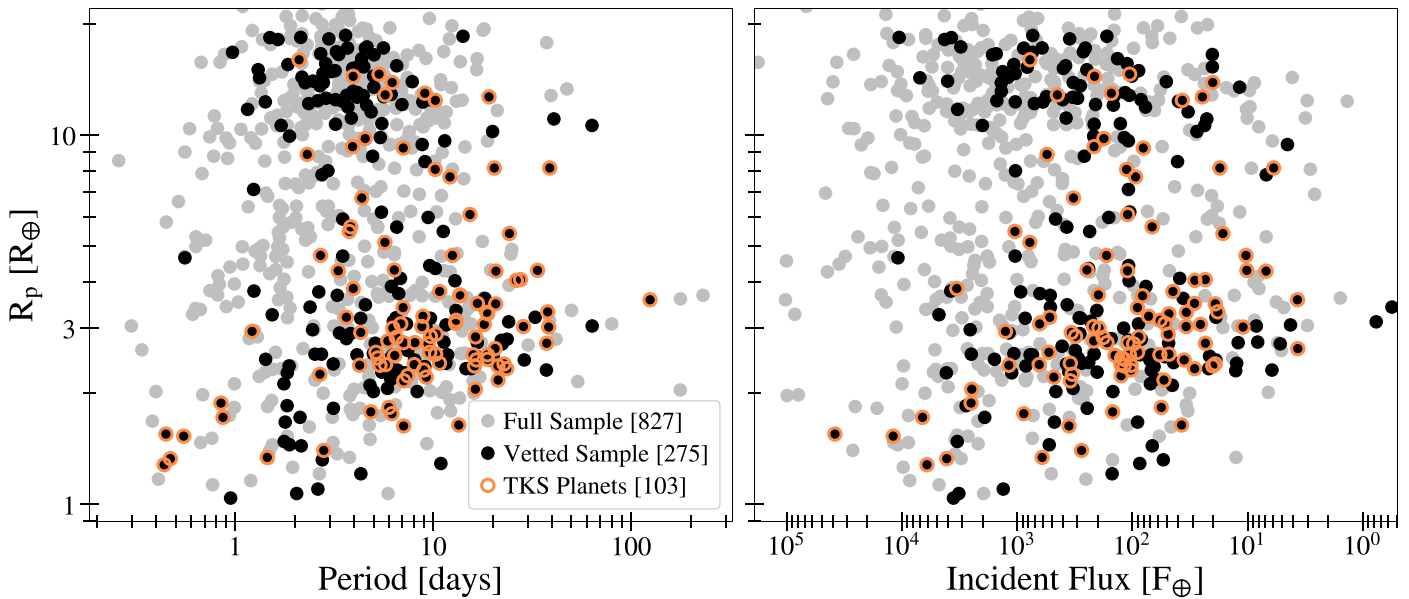


Figure 8. Planet sizes of TOIs plotted vs. period (left) and incident flux (right). Gray symbols represent all TOIs with decl. $\delta > = -30^\circ$ and Gaia RUWE metric < 2 . Black symbols include all TOIs that passed every vetting step, as discussed in Section 3. The final selected TESS-Keck Survey sample, which is highlighted in orange, includes 86 unique systems with a total of 103 planets.

brighter targets available for selection were almost always selected (Figure 6(a)), because brighter targets are cheaper and therefore typically more highly ranked. Moreover, most TKS targets are brighter than $V=12$, with the exception of one or two hand-selected targets.

Figure 7 shows various host star properties for the TKS sample. Of the selected 86 targets, 51 are solar-type stars, which are defined here as any star with an effective temperature within ± 500 K of that of the Sun. There are very few hot stars, most likely due to the rapid rotation of stars past the Kraft break (occurring near ~ 6250 K). Stellar masses and metallicities appear clustered around solar-like values (Figure 7, right), as expected from the effective temperature distribution. Fortunately, the diverse range in metallicity was a natural outcome

of the selection process. On the other hand, cool low-mass stars were selected less often, because they are fainter and therefore more expensive. Therefore, in order to partially avoid this bias, TOI 1467 and TOI 1801 were added as high-priority targets for SC1E and ended up being the two coolest stars in the TKS sample (with $T_{\text{eff}} \leq 4000$ K).

Figure 8 shows the sample of 103 planets in 86 systems selected for the TESS-Keck Survey. Planet properties are slightly biased toward sub-Jovian planets, which was expected since all but TKS Evolved (SC4) preferentially selected smaller planets. In fact, the sample includes 71 planets smaller than $\leq 4 R_{\oplus}$ that span over four orders of magnitude in incident flux, including a few that receive fluxes similar to that received by the Earth. Targets for the habitable zone science case are cooler than

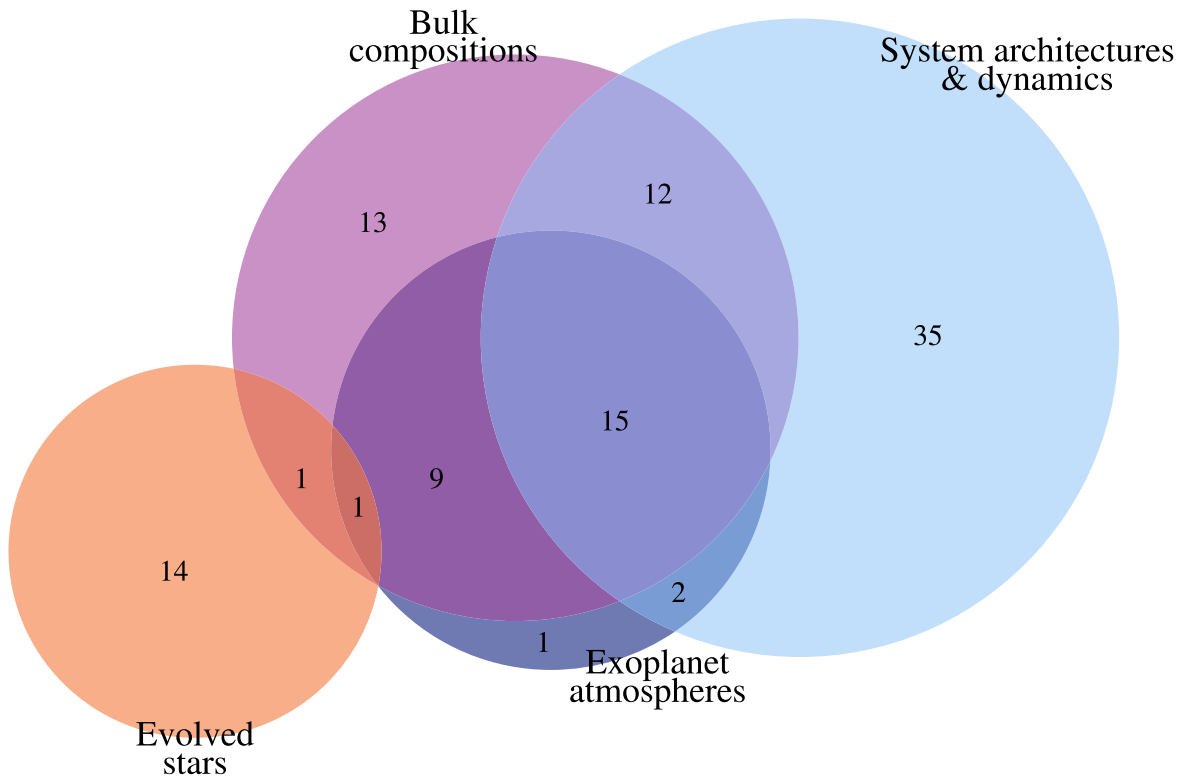


Figure 9. Venn diagram of the selected planet sample divided into the four TKS science cases: (1) bulk compositions, (2) system architectures & dynamics, (3) exoplanet atmospheres, and (4) evolved stars. Numbers indicate the number of *planets* belonging to each unique set of science cases, where total numbers include 51 planets for SC1, 64 planets for SC2, 28 planets for SC3, and 16 planets for SC4. The entire sample will be used for investigating any star–planet correlations (SCIE), characterizing properties of TKS host stars (TA), as well as exploring Doppler noise contributions and/or dependencies (TB).

the majority of small planets with measured densities and are therefore useful for exploring how planet properties change with decreasing incident flux. The TKS sample also includes a handful of planets at the opposite extreme, on orbits with sub-day periods, and therefore presumably with little-to-no remaining atmosphere.

While not unexpected, the strong overlap between the broad TKS science themes is remarkable. Figure 9 shows a Venn diagram of the planet sample by science case, and Figure 10 shows the samples in host star and planet parameter spaces. The full TKS sample demonstrates the proof of concept for the unique target selection process. Most notably, the large number of interdisciplinary targets that were automatically identified through the algorithm emphasizes the value of applying such target selection techniques. This demonstrates its potential usefulness for other large surveys in the future that face similar challenges related to target selection processes, especially for collaborations with sub-teams and/or overlapping science cases.

The complete TKS sample selected by the algorithm is provided in Tables 3 including the science case(s) for each target. Most notably, the highest-priority targets within the TKS sample (i.e., targets prioritized by the most science cases) have been or will be highlighted by early TKS single-object publications. An example is the galactic thick disk multiplanet system with an ultra-short-period planet, TOI 561 (Weiss et al. 2021). Other examples include warm Jupiters with only one or two transits that represent a means to extend beyond the planet demographic for which the TESS mission is optimized (Dalba et al. 2020, Dalba et al. submitted). More recently, TKS published precise ($>5\sigma$) masses for *nine* sub-Neptunes in four multiplanet TESS systems, including TOI-509 (HD 63935; Scarsdale et al. 2021), TOI-1246 (Turtelboom et al. submitted),

TOI-1255 (HIP-97166; MacDougall et al. 2021), and TOI-1339 (HD 191939; Lubin et al. 2022). The entire TKS sample provided in this paper has not been modified since August 21, 2020, but is still subject to change as the survey continues.

7. Conclusions

In this paper, we have presented the science cases and target selection process for the TESS-Keck Survey, a large program using Keck/HIRES to confirm and characterize planets discovered with TESS.

Our main conclusions are as follows:

1. The TESS-Keck survey was designed to measure precise ($>5\sigma$) masses for ~ 100 planets using an allocation of ~ 100 nights over four semesters. TKS will leverage this new population of transiting exoplanets orbiting bright, nearby stars to address four main science themes: (1) the bulk compositions of small planets; (2) dynamical temperatures and system architectures; (3) a larger, more refined sample for future atmospheric studies; and (4) planets orbiting evolved stars (Section 2.1).
2. We have developed open-source software for a fully automated and reproducible target selection procedure, which can be adapted for and used by other surveys (Section 5.2). By providing a set of science programs with unique selection criteria and prioritization metrics, the ranking algorithm will randomly select programs and program targets until the allocated resources are exhausted.
3. A total of 86 targets were selected by the prioritization algorithm for the final TKS sample (Section 6). The majority of TKS hosts are brighter ($V < 12$), solar-like

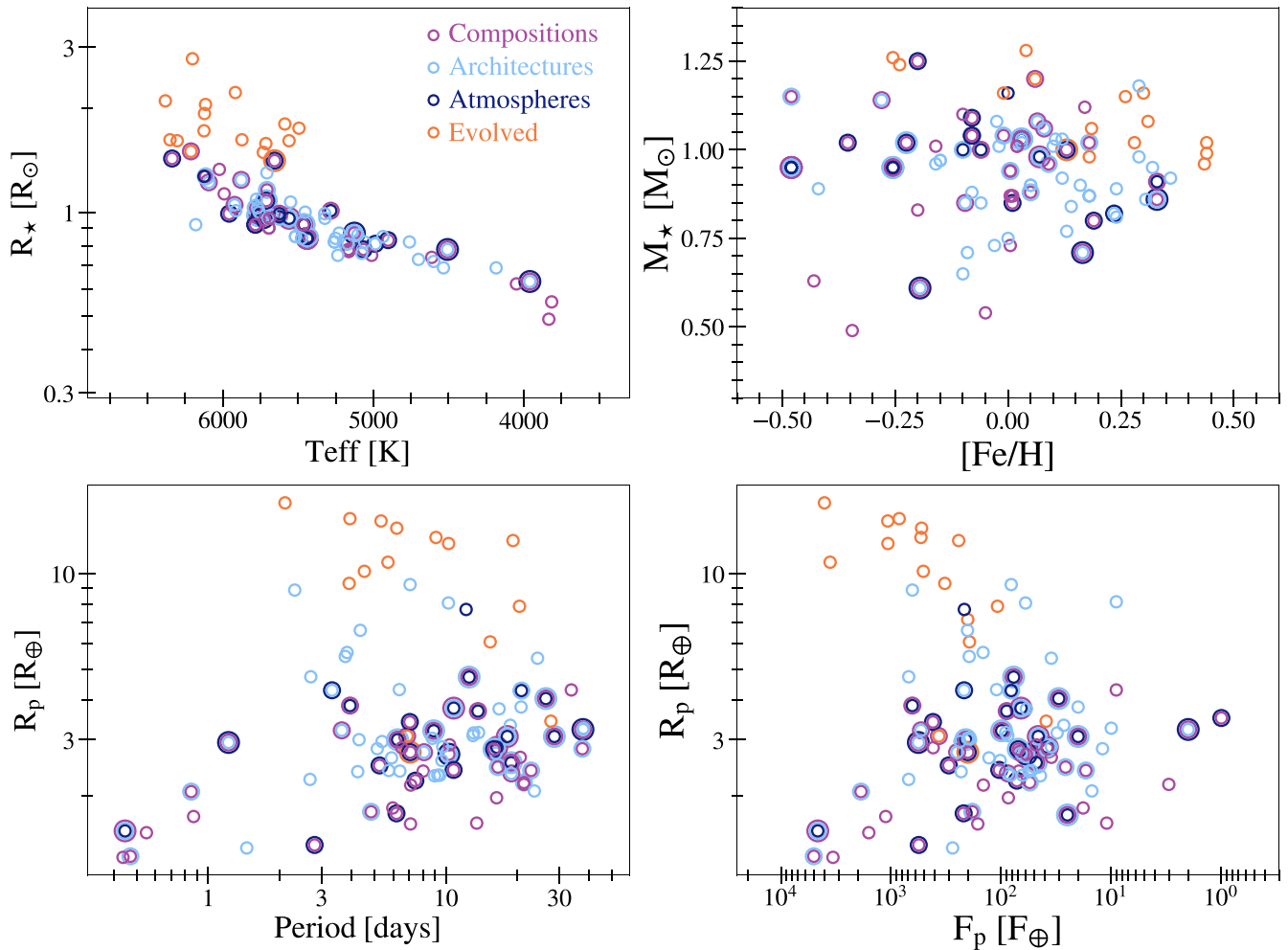


Figure 10. Same as Figures 7 and 8, but now only showing the selected TKS sample. Markers are colored by the four TKS science cases, where concentric rings represent higher-priority targets that address multiple science cases.

main-sequence stars with effective temperatures, $4500\text{ K} \leq T_{\text{eff}} < 6000\text{ K}$, at a wide range of metallicities ($-0.5 < [\text{Fe}/\text{H}] < 0.5$). With the exceptions of hand-selected, high-priority targets for the obliquity and stellar activity programs, most stars have modest rotation and activity levels (Figures 6, 7, and 10).

4. The final TKS planet population comprises 103 transiting planets in a rich diversity of system configurations (Section 6, Tables 3–5). The selected sample has 71 small planets ($R_p \leq 4 R_{\oplus}$) with incident fluxes that span nearly five orders of magnitude, including a few that are in or near the habitable zone of their host star (Figures 6, 8, and 10).

The target selection presented here is the first in a series of papers presenting ensemble results from the TESS-Keck Survey. Future planned catalogs include homogeneous stellar properties, exoplanet masses and dynamical architectures of planetary systems observed by the TESS Mission. The target prioritization software presented in this paper is publicly available on GitHub⁵³ as the v1.1.0 release, which is archived on Zenodo (Chontos 2021) and currently designed to reproduce the enclosed TKS target sample. However, the selection algorithm can be generalized and applied in other

large collaborations or surveys that require a balance of multiple science interests within a given allocation.

This paper is based on data collected by the TESS mission. Funding for the TESS mission is provided by NASA’s Science Mission Directorate. We acknowledge the use of public TESS data from pipelines at the TESS Science Office and at the TESS Science Processing Operations Center. Resources supporting this work were provided by the NASA High-End Computing (HEC) Program through the NASA Advanced Supercomputing (NAS) Division at Ames Research Center for the production of the SPOC data products. This research has made use of the Exoplanet Follow-up Observation Program website, which is operated by the California Institute of Technology, under contract with the National Aeronautics and Space Administration under the Exoplanet Exploration Program.

We recognize and acknowledge the cultural role and reverence that the summit of Maunakea has within the indigenous Hawaiian community. We are deeply grateful to have the opportunity to conduct observations from this mountain. We thank all the observers who spent time collecting data over the many years at Keck/HIRES. We gratefully acknowledge the efforts and dedication of the Keck Observatory staff for support of HIRES and remote observing. We thank the University of California and Google for supporting Lick Observatory and the UCO staff for

⁵³ sort-a-survey: <https://github.com/ashleychontos/sort-a-survey/>.

their dedicated work scheduling and operating the telescopes of Lick Observatory.










We are grateful to the time assignment committees of the University of California, University of Hawai'i, the California Institute of Technology, and NASA for supporting the TESS-Keck Survey with observing time at Keck Observatory and on the Automated Planet Finder. We thank NASA for funding associated with our Key Strategic Mission Support project. We thank Ken and Gloria Levy, who supported the construction of the Levy Spectrometer on the Automated Planet Finder.






























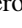













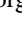






A.C., J.M.A.M., R.A.R., A.B., and A.M. acknowledge support from the National Science Foundation through the Graduate Research Fellowship Program (DGE 1842402, DGE 1842400, DGE 1745301, DGE 1745301, DGE 1752814). J.M.A.M. also acknowledges the LSSTC Data Science Fellowship Program, which is funded by LSSTC, NSF Cybertraining Grant No. 1829740, the Brinson Foundation, and the Moore Foundation; his participation in the program has benefited this work. T.F. acknowledges support from the University of California President's Postdoctoral Fellowship Program. D.H. acknowledges support from the Alfred P. Sloan Foundation, the National Aeronautics and Space Administration (80NSSC18K1585, 80NSSC19K0379), and the National Science Foundation (AST-1717000). I.J.M.C. acknowledges support from the NSF through grant AST-1824644. C.D.D. acknowledges the support of the Hellman Family Faculty Fund, the Alfred P. Sloan Foundation, the David & Lucile Packard Foundation, and the National Aeronautics and Space Administration via the TESS Guest Investigator Program (80NSSC18K1583). E.A.P. acknowledges the support of the Alfred P. Sloan Foundation. L.M.W. is supported by the Beatrice Watson Parent Fellowship and NASA ADAP Grant 80NSSC19K0597. P.D. acknowledges support from a National Science Foundation Astronomy and Astrophysics Postdoctoral Fellowship under award AST-1903811. S.G. acknowledges support from NASA FINESST Grant 80NSSC20K1549. E. E-B. acknowledges financial support from the European Union and the State Agency of Investigation of the Spanish Ministry of Science and Innovation (MICINN) under the grant PRE2020-093107 of the Pre-Doc Program for the Training of Doctors (FPI-SO) through FSE funds.

facility MAST, TESS, Keck I: HIRES.

Software: All code used in this paper is available at <https://github.com/ashleychontos/sort-a-survey>, with the archived version associated with this paper available at Chontos (2021). We made use of the following publicly available Python modules: *astroquery*, *exoplanet* (Foreman-Mackey 2019), *evolstate* (Huber 2017; Berger et al. 2018), and *tesspoint*.

ORCID iDs

Ashley Chontos  <https://orcid.org/0000-0003-1125-2564>
 Joseph M. Akana Murphy  <https://orcid.org/0000-0001-8898-8284>
 Mason G MacDougall  <https://orcid.org/0000-0003-2562-9043>
 Tara Fetherolf  <https://orcid.org/0000-0002-3551-279X>
 Judah Van Zandt  <https://orcid.org/0000-0002-4290-6826>
 Ryan A. Rubenzahl  <https://orcid.org/0000-0003-3856-3143>
 Corey Beard  <https://orcid.org/0000-0001-7708-2364>
 Daniel Huber  <https://orcid.org/0000-0001-8832-4488>
 Natalie M. Batalha  <https://orcid.org/0000-0002-7030-9519>

Courtney D. Dressing  <https://orcid.org/0000-0001-8189-0233>
 Benjamin Fulton  <https://orcid.org/0000-0003-3504-5316>
 Andrew W. Howard  <https://orcid.org/0000-0001-8638-0320>
 Howard Isaacson  <https://orcid.org/0000-0002-0531-1073>
 Stephen R. Kane  <https://orcid.org/0000-0002-7084-0529>
 Erik A. Petigura  <https://orcid.org/0000-0003-0967-2893>
 Paul Robertson  <https://orcid.org/0000-0003-0149-9678>
 Arpita Roy  <https://orcid.org/0000-0001-8127-5775>
 Lauren M. Weiss  <https://orcid.org/0000-0002-3725-3058>
 Aida Behmard  <https://orcid.org/0000-0003-0012-9093>
 Fei Dai  <https://orcid.org/0000-0002-8958-0683>
 Paul A. Dalba  <https://orcid.org/0000-0002-4297-5506>
 Steven Giacalone  <https://orcid.org/0000-0002-8965-3969>
 Michelle L. Hill  <https://orcid.org/0000-0002-0139-4756>
 Jack Lubin  <https://orcid.org/0000-0001-8342-7736>
 Andrew Mayo  <https://orcid.org/0000-0002-7216-2135>
 Teo Močnik  <https://orcid.org/0000-0003-4603-556X>
 Lee J. Rosenthal  <https://orcid.org/0000-0001-8391-5182>
 Nicholas Stursdale  <https://orcid.org/0000-0003-3623-7280>
 Emma V. Tuttleboom  <https://orcid.org/0000-0002-1845-2617>
 George R. Ricker  <https://orcid.org/0000-0003-2058-6662>
 Roland Vanderspek  <https://orcid.org/0000-0001-6763-6562>
 David W. Latham  <https://orcid.org/0000-0001-9911-7388>
 Sara Seager  <https://orcid.org/0000-0002-6892-6948>
 Joshua N. Winn  <https://orcid.org/0000-0002-4265-047X>
 Jon M. Jenkins  <https://orcid.org/0000-0002-4715-9460>
 Samuel N. Quinn  <https://orcid.org/0000-0002-8964-8377>
 Natalia M. Guerrero  <https://orcid.org/0000-0002-5169-9427>
 Karen A. Collins  <https://orcid.org/0000-0001-6588-9574>
 David R. Ciardi  <https://orcid.org/0000-0002-5741-3047>
 Avi Shporer  <https://orcid.org/0000-0002-1836-3120>
 Robert F. Goetze  <https://orcid.org/0000-0003-1748-5975>
 Alan M. Levine  <https://orcid.org/0000-0001-8172-0453>
 Eric B. Ting  <https://orcid.org/0000-0002-8219-9505>
 Allyson Bieryla  <https://orcid.org/0000-0001-6637-5401>
 Kevin I. Collins  <https://orcid.org/0000-0003-2781-3207>
 John F. Kielkopf  <https://orcid.org/0000-0003-0497-2651>
 Khalid Barkaoui  <https://orcid.org/0000-0003-1464-9276>
 Paul Benni  <https://orcid.org/0000-0001-6981-8722>
 Emma Esparza-Borges  <https://orcid.org/0000-0002-2341-3233>
 Dennis M. Conti  <https://orcid.org/0000-0003-2239-0567>
 Matthew J. Hooton  <https://orcid.org/0000-0003-0030-332X>
 Taiki Kagetani  <https://orcid.org/0000-0002-5331-6637>
 Giuseppe Marino  <https://orcid.org/0000-0001-8134-0389>
 Bob Massey  <https://orcid.org/0000-0001-8879-7138>
 Felipe Murgas  <https://orcid.org/0000-0001-9087-1245>
 Richard P. Schwarz  <https://orcid.org/0000-0001-8227-1020>
 Chris Stockdale  <https://orcid.org/0000-0003-2163-1437>
 Gavin Wang  <https://orcid.org/0000-0003-3092-4418>
 Justin M. Wittrock  <https://orcid.org/0000-0002-7424-9891>
 Yujie Zou  <https://orcid.org/0000-0002-5609-4427>

References

- Addison, B. C., Wright, D. J., Nicholson, B. A., et al. 2021, *MNRAS*, 502, 3704
 Armstrong, D. J., & consortium, N. 2021, The NCORES Program: HARPS Follow-up of TESS Discoveries Near the Photoevaporation Gap, Zenodo, doi:10.5281/zenodo.5126920

- Armstrong, D. J., Lopez, T. A., Adibekyan, V., et al. 2020, *Natur*, **583**, 39
- Batalha, N. E., Lewis, T., Fortney, J. J., et al. 2019, *ApJL*, **885**, L25
- Batalha, N. M., Borucki, W. J., Bryson, S. T., et al. 2011, *ApJ*, **729**, 27
- Batalha, N. M., Rowe, J. F., Bryson, S. T., et al. 2013, *ApJS*, **204**, 24
- Batygin, K., Morbidelli, A., & Tsiganis, K. 2011, *A&A*, **533**, A7
- Belokurov, V., Penoyre, Z., Oh, S., et al. 2020, *MNRAS*, **496**, 1922
- Berger, T. A., Huber, D., Gaidos, E., & van Saders, J. L. 2018, *ApJ*, **866**, 99
- Berger, T. A., Huber, D., van Saders, J. L., et al. 2020, *AJ*, **159**, 280
- Borucki, W. J., Koch, D. G., Basri, G., et al. 2011a, *ApJ*, **736**, 19
- Borucki, W. J., Koch, D. G., Basri, G., et al. 2011b, *ApJ*, **728**, 117
- Burke, C. J., Bryson, S. T., Mullally, F., et al. 2014, *ApJS*, **210**, 19
- Burke, C. J., Levine, A., Fausnaugh, M., et al. 2020, TESS-Point: High precision TESS pointing tool, Astrophysics Source Code Library, ascl:2003.001
- Chaplin, W. J., Kjeldsen, H., Bedding, T. R., et al. 2011, *ApJ*, **732**, 54
- Chen, J., & Kipping, D. 2017, *ApJ*, **834**, 17
- Chontos, A. 2021, ashleychontos/sort-a-survey: Chontos+2021, vv1.1.0, Zenodo, doi:10.5281/zenodo.5204725
- Chontos, A., Huber, D., Berger, T. A., et al. 2021, *ApJ*, **922**, 229
- Chontos, A., Huber, D., Latham, D. W., et al. 2019, *AJ*, **157**, 192
- Chubak, C., Marcy, G., Fischer, D. A., et al. 2012, arXiv:1207.6212
- Cloutier, R., Eastman, J. D., Rodriguez, J. E., et al. 2020, *AJ*, **160**, 3
- Coughlin, J. L., Mullally, F., Thompson, S. E., et al. 2016, *ApJS*, **224**, 12
- Crossfield, I. J. M., & Kreidberg, L. 2017, *AJ*, **154**, 261
- Dai, F., Howard, A. W., Batalha, N. M., et al. 2021, *AJ*, **162**, 62
- Dai, F., Roy, A., Fulton, B., et al. 2020, *AJ*, **160**, 193
- Dalba, P. A., Gupta, A. F., Rodriguez, J. E., et al. 2020, *AJ*, **159**, 241
- Dawson, R. I., & Johnson, J. A. 2012, *ApJ*, **756**, 122
- Dreizler, S., Crossfield, I. J. M., Kossakowski, D., et al. 2020, *A&A*, **644**, A127
- Evans, D. F. 2018, *RNAAS*, **2**, 20
- Evans, D. W., Riello, M., De Angeli, F., et al. 2018, *A&A*, **616**, A4
- Fabrycky, D., & Tremaine, S. 2007, *ApJ*, **669**, 1298
- Ford, E. B., & Rasio, F. A. 2008, *ApJ*, **686**, 621
- Foreman-Mackey, D. 2019, Exoplanet: Probabilistic Modeling of Transit or Radial Velocity Observations of Exoplanets, Astrophysics Source Code Library, ascl:1910.005
- Fressin, F., Torres, G., Charbonneau, D., et al. 2013, *ApJ*, **766**, 81
- Fulton, B. J., & Petigura, E. A. 2018, *AJ*, **156**, 264
- Fulton, B. J., Petigura, E. A., Howard, A. W., et al. 2017, *AJ*, **154**, 109
- Gaia Collaboration, Brown, A. G. A., Vallenari, A., et al. 2018, *A&A*, **616**, A1
- Gaia Collaboration, Prusti, T., de Bruijne, J. H. J., et al. 2016, *A&A*, **595**, A1
- Gardner, J. P., Mather, J. C., Clampin, M., et al. 2006, *SSRv*, **123**, 485
- Ginzburg, S., Schlichting, H. E., & Sari, R. 2018, *MNRAS*, **476**, 759
- Goldreich, P., & Schlichting, H. E. 2014, *AJ*, **147**, 32
- Grunblatt, S. K., Huber, D., Gaidos, E., et al. 2018, *ApJL*, **861**, L5
- Guerrero, N. M., Seager, S., Huang, C. X., et al. 2021, *ApJS*, **254**, 39
- Gupta, A., & Schlichting, H. E. 2019, *MNRAS*, **487**, 24
- Gupta, A., & Schlichting, H. E. 2020, *MNRAS*, **493**, 792
- Howard, A. W., Marcy, G. W., Bryson, S. T., et al. 2012, *ApJS*, **201**, 15
- Huang, C. X., Burt, J., Vanderburg, A., et al. 2018, *ApJL*, **868**, L39
- Huang, C. X., Vanderburg, A., Pál, A., et al. 2020a, *RNAAS*, **4**, 204
- Huang, C. X., Vanderburg, A., Pál, A., et al. 2020b, *RNAAS*, **4**, 206
- Huber, D. 2017, Isoclassify, v1.2, Zenodo, doi:10.5281/zenodo.573372
- Huber, D., Chaplin, W. J., Chontos, A., et al. 2019, *AJ*, **157**, 245
- Hut, P. 1981, *A&A*, **99**, 126
- Isaacson, H., & Fischer, D. 2010, *ApJ*, **725**, 875
- Jenkins, J. M., Twicken, J. D., McCauliff, S., et al. 2016, *Proc. SPIE*, **9913**, 99133E
- Johnson, J. A., Bowler, B. P., Howard, A. W., et al. 2010, *ApJL*, **721**, L153
- Johnson, J. A., Fischer, D. A., Marcy, G. W., et al. 2007, *ApJ*, **665**, 785
- Johnson, J. A., Morton, T. D., & Wright, J. T. 2013, *ApJ*, **763**, 53
- Kabath, P., Carleo, I., Guenther, E., et al. 2021, Spectroscopic Follow-up of TESS Candidates with KESPRINT 1.5-3-m telescopes Network, Zenodo, doi:10.5281/zenodo.5136646
- Kempton, E. M. R., Bean, J. L., Louie, D. R., et al. 2018, *PASP*, **130**, 114401
- Kipping, D. M., Dunn, W. R., Jasinski, J. M., & Manthri, V. P. 2012, *MNRAS*, **421**, 1166
- Kolbl, R., Marcy, G. W., Isaacson, H., & Howard, A. W. 2015, *AJ*, **149**, 18
- Lacedelli, G., Malavolta, L., Borsato, L., et al. 2021, *MNRAS*, **501**, 4148
- Léger, A., Grasset, O., Fegley, B., et al. 2011, *Icar*, **213**, 1
- Li, J., Tenenbaum, P., Twicken, J. D., et al. 2019, *PASP*, **131**, 024506
- López-Morales, M., Haywood, R. D., Coughlin, J. L., et al. 2016, *AJ*, **152**, 204
- Lubin, J., Van Zandt, J., Holcomb, R., et al. 2022, *AJ*, **163**, 101
- Luhn, J. K., Bastien, F. A., Wright, J. T., et al. 2019, *AJ*, **157**, 149
- Luhn, J. K., Wright, J. T., Howard, A. W., & Isaacson, H. 2020, *AJ*, **159**, 235
- Lundkvist, M. S., Kjeldsen, H., Albrecht, S., et al. 2016, *NatCo*, **7**, 11201
- MacDougall, M. G., Petigura, E. A., Angelo, I., et al. 2021, *AJ*, **162**, 265
- Mordasini, C. 2018, in Planetary Population Synthesis, ed. H. J. Deeg & J. A. Belmonte (Berlin: Springer), **143**
- Mordasini, C., van Boekel, R., Mollière, P., Henning, T., & Benneke, B. 2016, *ApJ*, **832**, 41
- Mulders, G. D., Mordasini, C., Pascucci, I., et al. 2019, *ApJ*, **887**, 157
- Mullally, F., Coughlin, J. L., Thompson, S. E., et al. 2015, *ApJS*, **217**, 31
- Owen, J. E., & Campos Estrada, B. 2020, *MNRAS*, **491**, 5287
- Owen, J. E., & Wu, Y. 2013, *ApJ*, **775**, 105
- Owen, J. E., & Wu, Y. 2017, *ApJ*, **847**, 29
- Petigura, E. A. 2015, PhD thesis, Univ. of California, Berkeley
- Petigura, E. A., Howard, A. W., & Marcy, G. W. 2013, *PNAS*, **110**, 19273
- Ricker, G. R., Winn, J. N., Vanderspek, R., et al. 2015, *JATIS*, **1**, 014003
- Rogers, L. A. 2015, *ApJ*, **801**, 41
- Rogers, L. A., & Seager, S. 2010, *ApJ*, **712**, 974
- Rowe, J. F., Coughlin, J. L., Antoci, V., et al. 2015, *ApJS*, **217**, 16
- Rubenzahl, R. A., Dai, F., Howard, A. W., et al. 2021, *AJ*, **161**, 119
- Scarsdale, N., Murphy, J. M. A., Batalha, N. M., et al. 2021, *AJ*, **162**, 215
- Schofield, M., Chaplin, W. J., Huber, D., et al. 2019, *ApJS*, **241**, 12
- Smith, J. C., Stumpe, M. C., Van Cleve, J. E., et al. 2012, *PASP*, **124**, 1000
- Stassun, K. G., Oelkers, R. J., Paegert, M., et al. 2019, *AJ*, **158**, 138
- Stumpe, M. C., Smith, J. C., Catanzarite, J. H., et al. 2014, *PASP*, **126**, 100
- Stumpe, M. C., Smith, J. C., Van Cleve, J. E., et al. 2012, *PASP*, **124**, 985
- Teske, J., Xuesong Wang, S., Wolfgang, A., et al. 2021, *ApJS*, **256**, 33
- Thompson, S. E., Coughlin, J. L., Hoffman, K., et al. 2018, *ApJS*, **235**, 38
- Twicken, J. D., Catanzarite, J. H., Clarke, B. D., et al. 2018, *PASP*, **130**, 064502
- Van Eylen, V., & Albrecht, S. 2015, *ApJ*, **808**, 126
- Van Eylen, V., Albrecht, S., Huang, X., et al. 2019, *AJ*, **157**, 61
- Villaver, E., Livio, M., Mustill, A. J., & Siess, L. 2014, *ApJ*, **794**, 3
- Weiss, L. M., Dai, F., Huber, D., et al. 2021, *AJ*, **161**, 56
- Weiss, L. M., & Marcy, G. W. 2014, *ApJL*, **783**, L6
- Winn, J. N. 2010, Exoplanets (Tucson, AZ: Univ of Arizona Press), **55**
- Wu, Y., & Lithwick, Y. 2011, *ApJ*, **735**, 109
- Yee, S. W., Petigura, E. A., & von Braun, K. 2017, *ApJ*, **836**, 77
- Yu, J., Huber, D., Bedding, T. R., & Stello, D. 2018, *MNRAS*, **480**, L48
- Zahn, J.-P. 1977, *A&A*, **57**, 383
- Zahn, J.-P. 1989, *A&A*, **220**, 112
- Zhou, G., Winn, J. N., Newton, E. R., et al. 2020, *ApJL*, **892**, L21
- Ziegler, C., Tokovinin, A., Briceño, C., et al. 2020, *AJ*, **159**, 19